

# Detection of organic carbon in Mars-analog paleosols with thermal and evolved gas analysis

Adrian P. Broz\*<sup>1</sup>, Joanna Clark<sup>2</sup>, Brad Sutter<sup>3</sup>, Doug W. Ming<sup>4</sup>, Briony Horgan<sup>5</sup>, Paul Douglas Archer Jr.<sup>3</sup> and Lucas C.R. Silva<sup>6,7</sup>

<sup>1</sup>Department of Earth Sciences, University of Oregon, Eugene, OR 97405

<sup>2</sup>Geocontrols Systems – Jacobs JETS Contract, NASA Johnson Space Center, Houston, TX, 77058

<sup>3</sup>Jacobs JETS Contract, NASA Johnson Space Center, Houston, TX 77058

<sup>4</sup>NASA Johnson Space Center, Houston, TX, 77058

<sup>5</sup>Department of Earth, Atmospheric and Planetary Science, Purdue University, IN, 47907

<sup>6</sup>Environmental Studies Program, Department of Geography, University of Oregon, Eugene, OR 97405

<sup>7</sup>Institute of Ecology and Evolution, University of Oregon, Eugene, OR 97405

\*Corresponding author, abroz@uoregon.edu

## Key points

- Trace amounts of organic carbon and organic fragments in Mars-analog paleosols were detected with thermal and evolved gas analysis
- The near-surface horizons of 30-million-year-old paleosols had significantly higher organic carbon content relative to deeper layers
- Radiocarbon dates of approximately 6-14 thousand years before present was consistent with late diagenetic additions of organic carbon

*This paper is a non-peer reviewed preprint submitted to EarthArXiv.*

33

**34 Abstract**

35 Ancient, buried soils, or paleosols, may have been preserved in the geological record on Mars, and are  
36 considered high-priority targets for biosignature investigation. Studies of paleosols on Earth that are  
37 similar in composition to putative martian paleosols can provide a reference frame for constraining their  
38 organic preservation potential on Mars. However, terrestrial paleosols typically preserve only trace  
39 amounts of organic carbon. Moreover, the study of terrestrial paleosols is complicated by diagenetic  
40 additions of organic carbon, which can confound interpretations of their organic preservation potential.  
41 The objectives of this study were a) to determine whether organic carbon in Mars-analog paleosols can be  
42 detected with thermal and evolved gas analysis, and b) constrain the age of organic carbon using  
43 radiocarbon ( $^{14}\text{C}$ ) dating. Oligocene (33 Ma) paleosols from Oregon were examined with an instrument  
44 similar to the Sample Analysis at Mars Evolved Gas Analysis (SAM-EGA) instrument onboard the Mars  
45 Science Laboratory *Curiosity* rover. Trace amounts of organic carbon and fragments of organic molecules  
46 were observed in all samples. Total organic carbon (TOC) ranged from 0.002 -  $0.032 \pm 0.006$  wt. %.  
47 Evolutions of organic fragments co-occurred with evolutions of  $\text{CO}_2$  from organic carbon decomposition.  
48 Like modern soils, the near-surface horizons of all paleosols had significantly higher TOC relative to  
49 subsurface layers. Radiocarbon dating revealed an organic carbon age of  $\sim 6,200 - 14,500$  years before  
50 present, suggesting there had been late diagenetic inputs of organic carbon. This work demonstrates that  
51 near-surface horizons of martian paleosols are a potential high priority location for *in-situ* biosignature  
52 investigation.

**53 Plain language summary**

54 Ancient, buried soils, or paleosols, may have been preserved in the geological record on Mars. On Earth,  
55 paleosols that are billions of years old contain past signs of life (biosignatures), and therefore paleosols on  
56 Mars are considered high-priority locations for biosignature investigation. One way to determine the  
57 biosignature preservation potential of possible martian paleosols is to examine organic carbon  
58 preservation in paleosols from Earth that resemble martian paleosols. The objectives of this work were a)  
59 determine whether organic carbon in Mars-analog paleosols can be detected by an instrument configured  
60 to operate like the Sample Analysis at Mars (SAM) Evolved Gas Analyzer (SAM-EGA) onboard  
61 *Curiosity* rover, and b) use radiocarbon dating to determine if samples contain recent/modern organic  
62 carbon. Trace amounts of organic carbon and fragments of organic molecules were observed in all  
63 samples. Like modern soils, the near-surface horizons of all paleosols had significantly higher amounts of  
64 organic carbon relative to subsurface layers. Radiocarbon dating revealed an organic carbon age of  
65  $\sim 6,200 - 14,500$  years before present, suggesting there had been additions of recent/modern organic  
66 carbon. These results demonstrate that near-surface horizons of putative martian paleosols are a potential  
67 high priority location for *in-situ* biosignature investigation.

68

69

70

71

72

73

74 **Introduction**

75 Paleosols are ancient, buried soils that are commonly lithified into sedimentary rocks. Terrestrial  
76 paleosols are a geological record of the atmospheric composition, climate, topography and organisms  
77 present before soil burial (Retallack, 2019). On Mars, paleosols, also known as weathering profiles, may  
78 have formed in sediments such as basaltic sand or volcanic ash that were subject to subaerial weathering  
79 by surface waters (Retallack, 2014; Amundson, 2018; Liu et al., 2021b; Ye and Michalski, 2021) and  
80 were subsequently buried and preserved in the geological record. Orbital remote sensing of the global  
81 martian surface has detected minerals within Noachian-age (4.1-3.7 Ga) layered sedimentary rocks that  
82 are consistent with precipitation-driven pedogenic weathering of mafic sediments (Carter et al., 2015;  
83 Bishop et al., 2018b; Loizeau et al., 2018). Noachian sedimentary rocks with spectral signatures of  
84 subaerial weathering have been detected in thousands of locations across the surface of Mars (Bishop et  
85 al., 2018b). One hypothesis is that these deposits are paleosols (Carter et al., 2015) which are the common  
86 products of pedogenic alteration followed by burial. Mounting evidence of global-scale aqueous alteration  
87 of the Martian surface during the Noachian (Carter et al., 2015; Liu et al., 2021a) suggests that  
88 pedogenesis could have been a critical process early in the planet's history. As such, paleosols have been  
89 recently named a high priority location for biosignature investigation (Bishop et al., 2018a) and Mars  
90 Sample Return (Beaty et al., 2019), but the biosignature preservation potential of paleosols with Mars-like  
91 mineralogy remains poorly constrained (Horgan, 2016).

92 On Earth, soils are highly habitable environments. Modern soils are teeming with microbial  
93 biomass, often averaging  $10^{10}$ – $10^{11}$  bacterial cells and  $10^3$  and  $10^4$  species per gram of soil (Raynaud and  
94 Nunan, 2014). Modern soils also contain more organic carbon than global vegetation and the atmosphere  
95 combined (Lehmann and Kleber, 2015; Dynarski et al., 2020). Similarly, Earth's oldest soils also appear  
96 to have been highly habitable environments. Many Precambrian ( $> 541$  Ma) paleosols contain organic  
97 carbon and other chemical biosignatures that are thought to be remnants of surface biomass (Matthewman  
98 et al., 2012; Kremer et al., 2017; Liivamägi et al., 2018; Broz, 2020). Furthermore, Archean ( $> 2$  Ga)  
99 paleosols contain filamentous organic carbon and organo-mineral complexes possibly derived from  
100 cyanobacterial mats on the soil surface (Rye and Holland, 2000; Watanabe et al., 2000).

101 Many terrestrial paleosols preserve only trace amounts of organic carbon, especially compared to  
102 modern soils, marine shales, and lacustrine rocks (Retallack, 2019). Organic carbon losses during  
103 diagenesis can reduce the organic carbon content of paleosols by up to two orders of magnitude relative to  
104 their modern soil counterparts (Broz, 2020). Severe losses of organic carbon are most common in  
105 paleosols that originally formed under oxidizing, well-drained conditions (Retallack and Mao, 2019). In  
106 general, oxidized paleosols typically contain only low amounts ( $< 0.1$  wt. %) of organic carbon (Broz,

107 2020). Diagenetic losses of organic carbon in oxidized terrestrial paleosols poses major challenges for  
108 detection of chemical and isotopic biosignatures preserved within the organic matter fraction. However,  
109 this is not the case for all paleosols. Those that originally formed under reducing conditions, such as  
110 Permian (~250 Ma) Histosols (poorly drained organic soils), preserve organic carbon with abundances >  
111 25 wt. % (Retallack and Krull, 1999), implying that redox state before burial may provide a first-order  
112 control on the preservation of organic carbon in ancient soils (Krull and Retallack, 2000).

113 An additional concern for the study of terrestrial paleosol organic matter is that diagenetic  
114 alterations ranging from groundwater alteration to precipitation-driven leaching of dissolved organic  
115 carbon can result in the addition of exogenous organic molecules, so caution is necessary for interpreting  
116 whether the organic fraction has indeed been “preserved” over geological time scales. In other words,  
117 terrestrial paleosols can be contaminated by organic molecules that were not original to the soil, thereby  
118 complicating efforts to interpret their biosignature preservation potential.

119 One way to constrain the biosignature preservation potential of putative paleosols on Mars is to  
120 examine the organic fraction of paleosols from Earth that share compositional and morphological  
121 similarities to layered sedimentary rocks on Mars. Examination of oxidized paleosols with Mars-like  
122 mineralogy can help determine if low amounts of organic molecules within natural pedogenic mineral  
123 matrices can be detected with Mars flight-analog instruments. Furthermore, cosmogenic nuclide dating of  
124 these analog paleosols can also identify potential diagenetic additions of organic carbon.

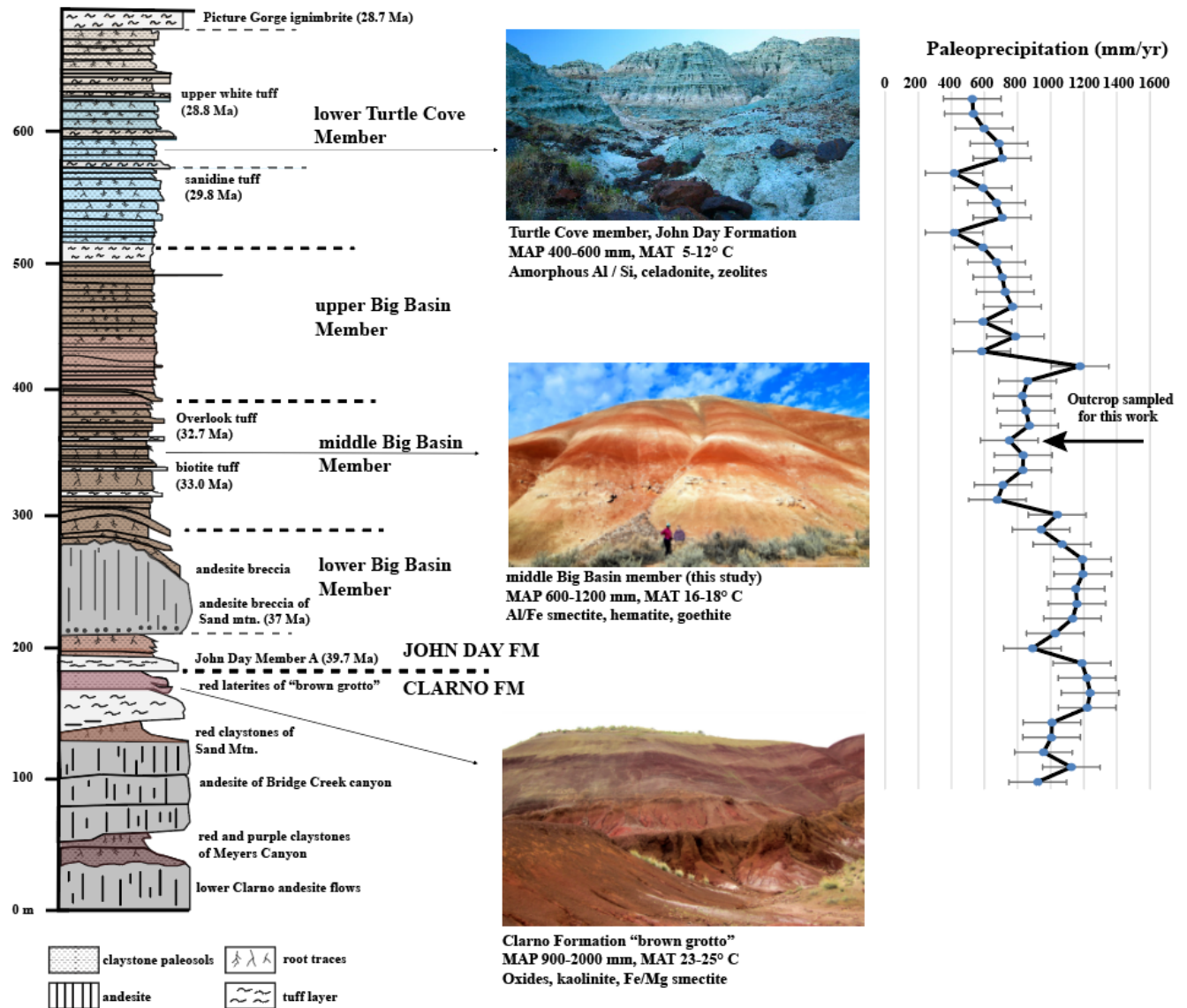
125 This study builds on and combines previous results from an established Mars-analog paleosol  
126 sequence (Broz et al., 2021a, 2021b). The focus here is to determine if organic molecules in oxidized  
127 paleosols are detectable with Mars flight-analog instrumentation, and to determine if there have been  
128 post-depositional additions of exogenous organic carbon. The objectives of this study were a) to  
129 determine whether organic carbon in ~30-million-year-old Mars-analog paleosols can be detected with  
130 thermal and evolved gas analysis, and b) constrain the age of organic carbon using radiocarbon ( $^{14}\text{C}$ )  
131 dating to identify late diagenetic additions of carbon.

132

### 133 **1.1 Paleosols at John Day Fossil Beds National Monument in eastern Oregon, USA**

134 Eocene and Oligocene (42-28 Ma) sedimentary rocks at John Day Fossil Beds National  
135 Monument in eastern Oregon are a thick sequence of volcanoclastic paleosols which altogether span over  
136 400 meters of vertical stratigraphy. (Bestland, 1997; Retallack et al., 2000; Horgan et al., 2012; Smith et  
137 al., 2018a). The paleosol sequence contains over 500 clay mineral-rich (30-95 wt. %) paleosols formed  
138 over ~15 Myr through the Eocene-Oligocene boundary (Figure 1) (Retallack et al., 2000; Horgan et al.,  
139 2018). Each of the individual profiles formed from pedogenic alteration of andesitic to rhyodacitic  
140 volcanic ash and/or tuff, followed by rapid burial via emplacement of an additional layer of tephra onto

141 the soil surface. This process of soil formation and burial repeated for nearly 15 million years, and as  
 142 such, the paleosol sequence provides a unique record of Cenozoic climate change in eastern Oregon  
 143 (Fremd, 1996). Changes in mineralogy throughout the paleosol sequence reflect the Eocene-Oligocene  
 144 cooling and drying of the climate (Bestland, 2002; Retallack et al., 2004).



146 **Figure 1. A sequence of Eocene and Oligocene (42-28 Ma) volcanioclastic paleosols in the Clarno and John Day**  
 147 **Formations, John Day Fossil Beds National Monument (after (Bestland, 1997) and (Sheldon et al., 2015)).**  
 148 Declining precipitation through the Eocene/Oligocene boundary is inferred from the mineralogy of paleosols from  
 149 the Clarno and John Day Formations. Paleoprecipitation estimates are from (Sheldon et al., 2015) who used an  
 150 equation relating molecular weathering ratios (Bases/alumina  $[CaO + MgO + Na_2O + K_2O / Al_2O_3]$ ) to mean annual  
 151 precipitation from a database of modern U.S. soils ( $r=0.79$ , standard error = 179 mm). The stratigraphic level of  
 152 paleosols analyzed in this work are indicated (black arrow, far right).  
 153

154           The Eocene (42-39 Ma) Clarno Formation represents the lowest and oldest unit of the Oregon  
155 paleosol sequence. The basal Clarno Formation is characterized by andesite flows interspaced with  
156 severely weathered paleosols with accumulations of kaolinite, Fe/Mg smectite and oxides (Oxisols and  
157 Ultisols in US soil taxonomy) which indicate tropical weathering conditions in the middle to late Eocene  
158 (Retallack et al., 2000). A particularly striking exposure of the late Eocene Clarno Formation at the  
159 “Brown Grotto” area of the Painted Hills is characterized by thick (~2-6 meter), repeated profiles of  
160 deeply weathered lateritic paleosols (Figure 1, bottom) that are similar to modern soils from Southern  
161 Mexico and Central America in climates that are subtropical and humid (Retallack et al., 2000).  
162 Stratigraphically above the Clarno Formation, the early Oligocene (~33 Ma) Big Basin Member of the  
163 John Day Formation is characterized by less intensely weathered paleosols (Alfisols and Inceptisols) that  
164 are rich in Al and Fe smectites such as nontronite and montmorillonite (Figure 1, middle). This middle  
165 unit represents a dramatic cooling and drying of the climate through the Eocene-Oligocene boundary.  
166 Overlying this unit of the paleosol sequence is the mid-late Oligocene (~28 Ma) Turtle Cove Member of  
167 the John Day Formation (Figure 1, top). The brown, green and celadon-colored paleosols of this unit are  
168 minimally weathered Aridisols (desert soils) and Andisols (amorphous-rich volcanic soils). Paleosols in  
169 this unit are characterized by accumulations of amorphous and nanocrystalline materials (e.g., allophane  
170 and imogolite), pedogenic calcite, and diagenetic celadonite (Horgan et al., 2012). There is a dramatic  
171 reduction in smectite content and absence of kaolinite which is consistent with weathering under a semi-  
172 arid to arid climate regime (Bestland, 2002). Finally, the entire paleosol sequence is capped by  
173 approximately 300 vertical meters of flood basalts from the Miocene (~16 Ma) Columbia River Basalt  
174 Group. Based on these mineralogical transitions, the Eocene paleosols with accumulations of kaolinite  
175 and oxides appear to reflect a subtropical and humid climate, while accumulations of nanophase  
176 aluminosilicates and amorphous phases in overlying paleosols indicate stepwise cooling and drying  
177 during the late Oligocene (Retallack et al., 2000).

178

## 179 **1.2 Pedogenic weathering on early Mars and comparisons to terrestrial paleosols**

180           From a global perspective, orbital remote sensing from Observatoire pour la Minéralogie, l'Eau,  
181 les Glaces, et l'Activité (OMEGA) and the Compact Reconnaissance Spectrometer at Mars (CRISM)  
182 instrument onboard the Mars Reconnaissance Orbiter provide the most compelling evidence of extensive  
183 pedogenic-like alteration across the surface of Mars. Potential weathering sequences have been detected  
184 in hundreds of locations across Noachian-age terrains, wherever these ancient rocks are not obscured by  
185 dust, sand, or overlying strata (Carter et al., 2015; Loizeau et al., 2018). OMEGA and CRISM have  
186 collectively gathered visible and near-infrared (VNIR) reflectance spectra of sedimentary deposits at  
187 Mawrth Vallis, Oxia Planum, Nili Fossae and other altered Noachian terrains. Some of these deposits,

188 such as layered outcrops at Mawrth Vallis, have spectral and stratigraphic similarities to terrestrial  
189 paleosol sequences (Horgan et al., 2012, 2018; Hays et al., 2017; Smith et al., 2018b; Poulet et al., 2020).  
190 Spectral refinements for CRISM images (e.g., (Viviano-Beck et al., 2014)) are allowing for identification  
191 of smaller-scale hydrated mineral deposits at Mawrth Vallis that facilitate a detailed reconstruction of  
192 possible geochemical environments on early Mars (Bishop et al., 2020).

193

#### 194 **Mawrth Vallis**

195 Previous work identified compositional and morphological similarities between the eastern  
196 Oregon paleosol sequence and layered outcrops at Mawrth Vallis (Horgan et al., 2012; Hays et al., 2017;  
197 Lantz et al., 2020; Smith and Horgan, 2021). The compositional stratigraphy at Mawrth Vallis has been  
198 interpreted as a paleosol sequence (Horgan et al., 2012) or a deep weathering profile (Liu et al., 2021a).  
199 Here, a ~200 m stack of layered sedimentary rocks has spectral signatures consistent with pedogenic-like  
200 alteration of mafic sediments (Horgan, 2013). The basal Fe/Mg smectite unit at Mawrth Vallis is  
201 dominated by spectral signatures of Fe/Mg smectite and is consistent with subaerial alteration under a  
202 warm and wet climate (Loizeau et al., 2015; Poulet et al., 2020). This basal unit transitions upward into a  
203 thin, ferrous-bearing clay unit that could have resulted from reducing conditions during subaerial  
204 weathering. This unit is overlain by layered rocks containing minerals consistent with formation in acidic  
205 and evaporitic geochemical settings, inferred from spectral signatures consistent with mixtures of smectite  
206 and jarosite (the “doublet” spectral feature) (Noe Dobrea et al., 2016; Danielson et al., 2019; Bishop et al.,  
207 2020). Stratigraphically higher, layered rocks with signatures of Al and Fe smectite are consistent with  
208 pedogenic weathering of volcanoclastic sediments under a semi-arid climate. Finally, the uppermost layers  
209 are characterized by accumulations of poorly consistent aluminosilicates, suggesting minimal or cool-  
210 climate alteration, which may represent the terminus of warm and wet conditions on early Mars (Bishop  
211 et al., 2020). The entire sequence is then capped by dark-toned sands and/or lava flows. One hypothesis  
212 to explain the stratigraphy at Mawrth Vallis is that it may represent the cooling and drying of the Martian  
213 climate during the mid to late Noachian (Bishop and Rampe, 2016; Bishop et al., 2020). Similarly, the  
214 Oregon paleosol sequence represents a transition from warm and wet conditions. The intensely weathered  
215 basal Clarno Formation paleosols transition upward into less-weathered semi-arid paleosols of the middle  
216 Big Basin Member, which contains both oxidized (red, brown) and reduced (yellow, black) paleosols.  
217 These are subsequently overlain by minimally weathered paleosols of the Oligocene Turtle Cove Member  
218 with accumulations of unweathered volcanic glass, amorphous colloids, calcite and hydrated silica which  
219 are thought to represent the terminus of warm and wet climate conditions in eastern Oregon. Terrestrial  
220 paleosols at the analog site have therefore been considered analogous to dioctahedral clay sequences on  
221 Mars. Layered rocks at Mawrth Vallis currently stand as the best example of a putative paleosol sequence

222 on Mars, but other locations, such as Jezero Crater, also show VNIR spectra consistent with subaerial  
223 alteration of mafic sediments.

224

### 225 **Jezero Crater**

226 Spectral signatures of Al-bearing clay minerals and/or silica deposits that could have formed in  
227 subaerial environments were detected approximately 3 km from the Perseverance rover landing site at  
228 Jezero Crater. Across Jezero's western delta and northern fans, there are strong and ubiquitous orbital  
229 detections of Al-bearing clay minerals and/or silica that could be either detrital or authigenic in origin  
230 (Horgan et al., 2020). The strongest signatures across the western delta are associated with features that  
231 resemble point bar deposits and are consistent with formation in subaerial and/or seasonally waterlogged  
232 paleoenvironments (Horgan et al., 2020). If authigenic in origin, these deposits could be subaerial  
233 paleoenvironments and include individual paleosol profiles. If targeted for *in-situ* examination by  
234 *Perseverance* rover, these deposits could provide critical information about the climate and duration of  
235 delta activity at Jezero Crater (Horgan et al., 2020). Similarly, terrestrial paleosols examined in this study  
236 formed from subaerial weathering of volcanoclastic sediments across alluvial terraces and have  
237 accumulated abundant Al clay minerals and amorphous silica (Bestland, 1997; Retallack et al., 2000). The  
238 mounting evidence of pedogenic-like processes on Mars emphasizes the need for study of paleosols from  
239 Earth to aid in future investigation and interpretation of sedimentary rocks on Mars.

240

### 241 **Terrestrial paleosols: Mineralogy and diagenesis**

242 The present study focuses on three paleosol profiles from the early Oligocene (33 Ma) Big Basin  
243 Member of the John Day Formation (Figure 1, middle). A detailed analysis of mineralogy and diagenetic  
244 alteration of these samples was previously performed (Broz et al., 2021a). X-ray diffraction evolved gas  
245 analysis and visible-near-infrared spectroscopy revealed high abundances (> 80 wt. %) of  
246 montmorillonite and nontronite with lesser amounts of hematite, zeolites, gypsum, and hydrated silica  
247 (Tables S4-S6). Diagenetic alterations previously observed in these samples included a) "burial  
248 gleization" of near-surface horizons, which is attributed to microbial reduction of Fe<sup>3+</sup> in near-surface  
249 horizons of paleosols, possibly during anaerobic decay of organic matter; b) dehydration of ferrous  
250 oxyhydroxides (goethite) to form fine-grained hematite; c) zeolitization to form clinoptilolite, possibly  
251 resulting from diagenetic recrystallization of a poorly crystalline smectite; and d) significant mechanical  
252 compaction to approximately 70% of the original soil thickness (Retallack et al., 2000).

253 Previously, there was no effort to examine the organic component of these paleosols, and the  
254 resulting influence of diagenesis on the organic fraction of Mars-analog paleosols is poorly understood.  
255 Examination of terrestrial paleosols with Mars flight-analog instruments such as evolved gas analysis

256 allows for a detailed characterization of the organic fraction (discussed below). This can help ascertain if  
257 diagenesis has resulted in severe losses of organic carbon in Mars-analog paleosols and determine if  
258 organic carbon that remains is detectable with analytical techniques relevant to Mars exploration.

259

### 260 **1.3 Sample Analysis at Mars (SAM) instrument onboard *Curiosity* Mars Rover**

261 The overall goal of the SAM instrument was to assess the potential for past habitability by  
262 characterizing the martian chemical and isotopic composition of the atmosphere and volatile-bearing  
263 surface materials (Mahaffy et al., 2012). The SAM instrument was integral in providing an understanding  
264 of organic materials and phases undetectable by CheMin (e.g., amorphous phases, low abundance  
265 phases). SAM heats scooped or drilled rock samples from  $\sim 30 - 870^\circ \text{C}$  at  $35^\circ \text{C min}^{-1}$ . Evolved gases  
266 produced from the thermal decomposition of volatile-bearing phases were analyzed by a quadrupole mass  
267 spectrometer (QMS), gas chromatograph columns for GCMS, or a tunable laser spectrometer (TLS)  
268 (Mahaffy et al., 2012). In evolved gas analysis (SAM-EGA) mode, SAM detected bulk gas evolution,  
269 whereas in gas chromatography-mass spectroscopy (SAM-GCMS) mode, SAM performed molecular  
270 separation and identification of organic molecules (Mahaffy et al., 2012; Eigenbrode et al., 2018). This  
271 study focused on SAM-EGA, so SAM-GCMS will not be further discussed. A comprehensive discussion  
272 on how organic molecules are detected with SAM- GCMS mode can be found in <sup>42</sup> and <sup>44</sup>.

273 Evolved gases and their release temperatures detected by SAM-EGA provide constraints on the  
274 mineralogy and organic content of samples in Gale Crater (Archer et al., 2014; Ming et al., 2014;  
275 Freissinet et al., 2015; Eigenbrode et al., 2018). The thermal decomposition of solid samples during  
276 SAM-EGA occurs during ramped heating, which releases volatile gases including  $\text{CO}_2$ ,  $\text{CO}$ ,  
277 hydrocarbons, and organic fragments (i.e.,  $\text{CH}_2$ ,  $\text{CH}_3$ ,  $\text{C}_2\text{H}_2$  and others) that are detected by the QMS. The  
278 intensity (relative abundance) of volatile release is plotted as a function of the release temperature,  
279 generating a time and temperature series of data for each volatile gas release. The volatile release peak  
280 temperature during sample decomposition depends on the thermodynamics of the reaction and can be  
281 used to constrain the composition of minerals and organic carbon in the sample (Archer et al., 2014), as  
282 well as to identify possible associations between minerals and organics (Mcadam et al., 2020b).

283 Additional future missions to Mars will also employ EGA-like analysis to search for organic  
284 molecules. The Mars Organic Molecule Analyzer (MOMA) onboard European Space Agency's ExoMars  
285 2022 *Rosalind Franklin* rover will use pyrolysis gas chromatography-mass spectrometry (GCMS) and  
286 laser desorption spectroscopy to search for biosignatures on Mars. Volatile gases thermally evolved from  
287 solid samples in the instrument oven will be separated by the GC and then analyzed individually with the  
288 MS (Goesmann et al., 2017) as is the case with SAM-GCMS, though MOMA will combine pyrolysis  
289 with laser desorption mass spectrometry, a less destructive technique that allows for identification of large

290 intact molecules and polar compounds. The *Rosalind Franklin* rover will land at Noachian –age (3.9 Ga)  
291 Oxia Planum which appears to be a westward extension of the lower parts of the stratigraphy observed at  
292 Mawrth Vallis (Ivanov et al., 2020; Loizeau et al., 2020). Like Mawrth Vallis, strong and ubiquitous  
293 spectral signatures of dioctahedral Al-rich clay minerals overlying Fe/ Mg clay minerals suggests Oxia  
294 Planum may host remnants of a thick (~200 m) deep weathering profile or paleosol sequence that the  
295 rover could encounter during its primary mission.

296

#### 297 **1.4 Previous detections of organic carbon with SAM-EGA**

298 Organic carbon has been detected in sedimentary rocks at Gale Crater with the SAM instrument  
299 using both QMS and GCMS (Ming et al., 2014; Rampe et al., 2014; Freissinet et al., 2015; Szopa et al.,  
300 2020). Abundances of reduced carbon were very low (< 1 wt. %) and restricted to three samples  
301 (Cumberland [CB], Confidence Hills [CH], and Mojave [MJ]). Though all CO<sub>2</sub> and CO detected to date is  
302 consistent with oxidized organic compounds, it is possible that contamination by the SAM-GCMS  
303 derivatization agent MTBSTFA could have resulted in these peaks. However, high-temperature (> 600°  
304 C) CO releases were consistent with endogenous oxidized martian organics. Additionally, chlorinated  
305 hydrocarbons (chlorobenzene [m/z 112], ~30 pmol) in the Cumberland drill sample and organo-sulfur  
306 compounds including thiophenes and thiols (~90 nmol) in the Mojave and Confidence Hills drill samples  
307 were identified in ~3.5 Ga mudstone, but the sources of these organic molecules was not constrained  
308 (Freissinet et al., 2015; Eigenbrode et al., 2018). Observation of dichlorobenzene and  
309 trichloromethylpropane in the CB sample at Yellowknife Bay could have been produced by chemical  
310 reactions between organic molecules and oxychlorines occurring in the SAM ovens. These chlorinated  
311 hydrocarbons could have been derived from organic carbon, either from an endogenous martian source  
312 and/or from meteoric infall (Fornaro et al., 2018; Szopa et al., 2020). Though organic carbon has been  
313 detected by SAM in numerous sedimentary deposits at Gale Crater, the source(s) of the organic molecules  
314 are not yet fully understood. Recent work has shown that organic salts such as Ca/ Mg oxalates and/or  
315 Ca/Mg acetates may be present in abundances of 1-2 wt. % in modern eolian sediments (Rocknest  
316 sample) as well as in ancient sedimentary rocks at Gale Crater (JK and CB samples) (Lewis et al., 2021).  
317 The accumulation of organic salts in eolian deposits suggests they may be a component of regional or  
318 global dust on Mars (Lewis et al., 2021).

319

#### 320 **1.5 Thermal analysis of organic carbon in modern soils and paleosols**

321 Thermal analysis techniques similar to SAM-EGA have been employed for understanding the  
322 nature and stability of organic matter in modern terrestrial soils, though at present there are only limited  
323 studies of paleosols (Noe Dobrea et al., 2016; Smith et al., 2018b). Past work has shown the thermal

324 decomposition of organic carbon (C) is related to organic carbon composition and particle size in both  
325 modern soils (Nelson and Baldock, 2005; Williams et al., 2018) and paleosols (Marin-Spiotta et al.,  
326 2014). In modern soils there is an inverse relationship between particle size and proportion of plant  
327 biopolymer-derived organic carbon (carbohydrates, lignin) and C from microbial biomass and/or  
328 metabolites (protein, aliphatic C) (Nelson and Baldock, 2005). Larger particle sizes are predominantly  
329 associated with labile remains of plant biopolymers, while the clay-size fraction hosts highly recalcitrant  
330 (stable) C compounds which include microbial biomarkers of n-C<sub>14</sub> alkanolic acid (Otto et al., 2005).  
331 Organic C associated with the clay-size fraction thermally decomposes at higher temperatures (~ 400 -  
332 450° C) compared to C associated with larger size fractions (~150° - 350° C) (Plante et al., 2011; Marin-  
333 Spiotta et al., 2014). Thus, the thermal stability of organic carbon associated with clay minerals and/ or  
334 persisting as microaggregates reflects increased resistance to oxidation (Williams et al., 2018) which is  
335 one factor among many contributing to stabilization over geological time scales (Bishop et al., 2013).  
336

### 337 **1.6 Preservation of organic matter in Archean paleosols**

338

339 Life on Earth has a long history with soil, and some of the oldest biosignatures of life on land are  
340 found in paleosols (Retallack, 2016; Homann et al., 2018; Finke et al., 2019). Transmission electron  
341 microscopy of the clay size fraction of an Archean (2.6 Ga) paleosol from South Africa showed organic  
342 carbon in association with surfaces and interlayer spaces of clay minerals, possibly derived from  
343 cyanobacterial mats (Watanabe et al., 2000). An Archean (~2.8 Ga) paleosol from Western Australia  
344 contained filamentous, carbon-rich microstructures with regular banding and consistent shape and size  
345 (Rye and Holland, 2000). These structures, which contain up to 0.1 wt. % carbon, have been interpreted  
346 as putative microfossils of methanogenic microbial mats living on the soil surface (Rye and Holland,  
347 2000). In both Archean paleosol examples, organic carbon was most concentrated in near-surface  
348 horizons. Near-surface layers of other Archean paleosols contain additional biosignatures such as  
349 isotopically light carbon (Retallack and Noffke, 2019) and sulfur (Nabhan et al., 2016). Early Archean  
350 (3.7 Ga) metasedimentary deposits from the Isua supercrustal belt in Greenland which have been  
351 considered putative paleosols (Retallack and Noffke, 2019) have  $\delta^{13}\text{C}_{\text{organic}}$  of -24.2 to -27.4 ‰ and show  
352 mineralogical evidence of subaerial acid-sulfate weathering, including abundant crystals of ripidolite  
353 interpreted to be pseudomorphs of the sulfate mineral kieserite. These appear to be grouped into a gypsic  
354 (By) horizon within a matrix of berthierine schist. Berthierine, a phyllosilicate in the serpentine group, is  
355 thought to have formed from metamorphism of a trioctahedral phyllosilicate like saponite (Retallack and  
356 Noffke, 2019), thus implying that early Archean Earth surface weathering may have been comparable to  
357 late Noachian surface weathering on Mars. The putative Greenland paleosol has been tortured by

358 metamorphism to amphibolite facies and thus any biogenic source for the isotopic fractionation and/or  
359 discrimination should be interpreted with caution. In any case, terrestrial paleosols provide compelling  
360 evidence of life's ancient relationship with surface environments on Earth, which appears to extend well  
361 back into the Archean (Gay and Grandstaff, 1980; Rye and Holland, 2000; Watanabe et al., 2000, 2004;  
362 Homann et al., 2018).

363         Though there appear to be similarities between the modes of weathering on the Early Earth and  
364 Mars (e.g., anoxic acid sulfate weathering), the use of Archean paleosols as Mars analogs is complicated  
365 by severe diagenetic overprinting that often obscures the original mineralogy and organic content of these  
366 ancient land surfaces. Younger, less altered paleosols are more suitable candidates for comparisons with  
367 putative paleosols on Mars, yet, as discussed below, these are also imperfect Mars analogs.

368

369

### 370 **1.7 Limitations of Cenozoic Mars-analog paleosols**

371         The Eocene-Oligocene (42-28 Ma) eastern Oregon paleosols are an incomplete Mars analog due  
372 to several fundamental differences. First, the source of organic carbon within the paleosols is primarily  
373 from microbial and/or plant biomass and represents a complex consortium of life above and within the  
374 soil profile. Therefore, the organic carbon component of these paleosols and the resulting preservation  
375 and degradation mechanisms may not be the same on Mars, but it is possible that putative paleosols at  
376 Mawrth Vallis have mineralogy analogous to terrestrial paleosols and thus have a similar mineralogical  
377 control on the fate of organic carbon. Nevertheless, the purpose of this study was not to determine the  
378 "inputs" of organic carbon in paleosols, but rather to observe the "outcomes" of life on land, e.g., if and  
379 how organic carbon is preserved across ancient surface environments.

380         A principal concern of this work was the assumption that all organic carbon in any lithified  
381 paleosol sample was endogenous (e.g., deposited during soil formation) and has subsequently been  
382 preserved for ~30 million years. This assumes no contribution from modern plants or microbes or  
383 diagenetic alterations which add exogenous organic carbon. For example, modern soils developing atop  
384 paleosol outcrops could have delivered exogenous organics to the underlying paleosols.

385         Another concern is the suite of common diagenetic alterations which alter paleosols, including  
386 zeolitization, illitization and burial decomposition of organic carbon which appear to have affected  
387 paleosols examined here to some degree (see Results). However, these are all assumed to remove  
388 endogenous organic carbon (Retallack, 2019), not deliver it. We tested the hypothesis that organic carbon  
389 is endogenous to paleosols by radiocarbon dating bulk samples (see Methods).

390         Large differences in age (Oligocene, [33 Ma] versus Noachian [4.1-3.7 Ga]) also have  
391 implications for diagenesis. John Day paleosols have experienced a range of minor to moderate diagenetic

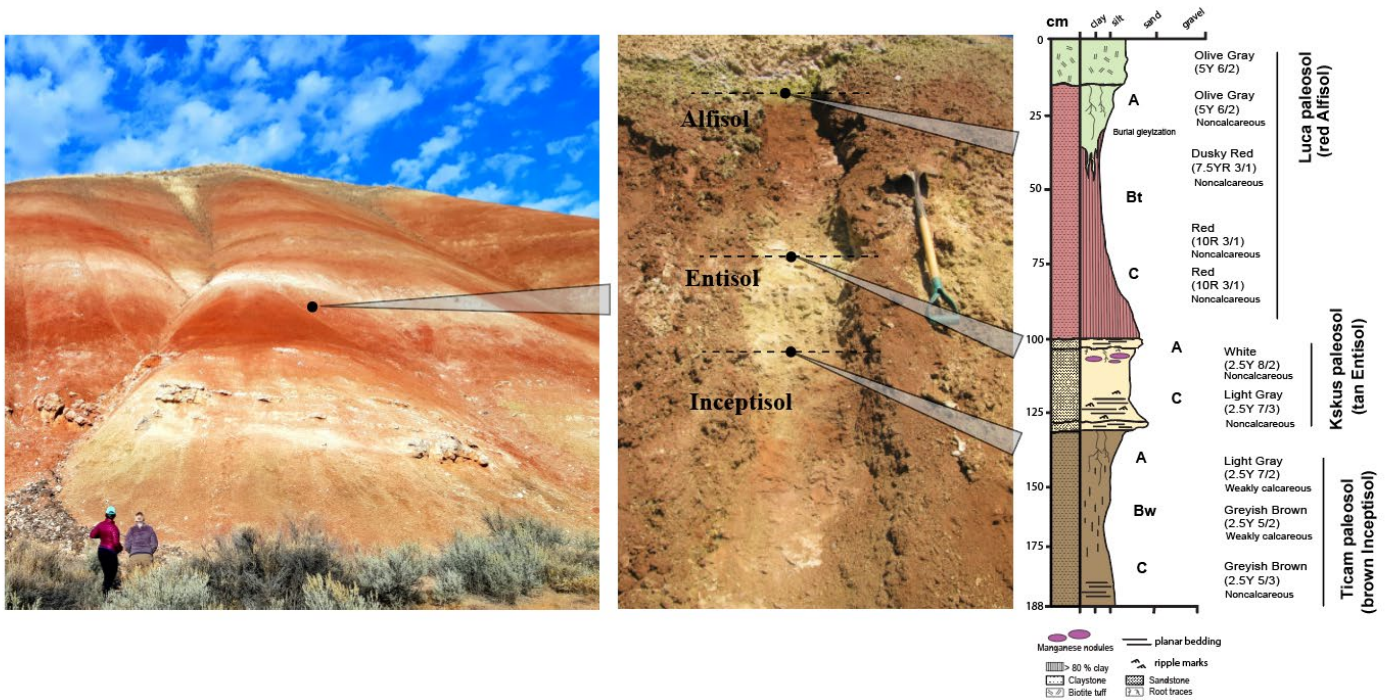
392 alteration including illitization of smectite, zeolitization and celadonization all resulting from alteration to  
393 clinoptilolite facies (Retallack et al., 2000; Horgan, 2016), but it is currently unclear if similar diagenetic  
394 alteration has affected potential paleosol sequences on Mars. There are also differences in the oxidation  
395 state of the atmosphere during subaerial weathering. The Oregon paleosols formed under a thoroughly  
396 oxidizing atmosphere but at present the oxidation state of an early Mars atmosphere is not well  
397 constrained (Ramirez et al., 2014). However, leaching of  $\text{Fe}^{2+}$  in putative martian paleosols at Mawrth  
398 Vallis has been inferred from spectral weathering indices and is consistent with an anoxic, reducing  
399 atmosphere during the Noachian (Liu et al., 2021a). Lastly, there are most likely differences in the pH of  
400 fluids participating in hydrolytic weathering of volcanoclastic sediments. The Oregon paleosols formed by  
401 pedogenic weathering with circumneutral-pH fluids, but subaerial alteration on Mars could have preceded  
402 with acidic,  $\text{H}_2\text{SO}_4$  and HCl-rich surface waters as a result of volcanic outgassing of  $\text{H}_2$  and  $\text{SO}_2$  (Liu et  
403 al., 2021a, 2021b). Despite these significant differences, the paleosol sequence from eastern Oregon  
404 offers a natural example to determine if organic carbon can be detected with thermal and evolved gas  
405 analysis techniques similar to SAM-EGA.

406

## 407 **1. Methods**

### 408 **2.1 Sample collection**

409 The paleosols examined in this study were collected from the Painted Hills Unit of the John Day  
410 Fossil Beds National Monument in eastern Oregon, USA. A previous study (Broz et al., 2021a)  
411 determined the mineralogy and diagenetic alteration of the same set of samples examined in the present  
412 study. Samples from three individual paleosols in vertical succession were collected approximately 7 km  
413 SW of the entrance to the Painted Hills unit of the John Day Formation (44.631105, -120.213107), in the  
414 Middle Big Basin Member of the John Day Formation, approximately 6 m above the local Eocene-  
415 Oligocene boundary (Figure 1, middle). Samples were chosen from this location because they were  
416 previously examined for mineralogy and diagenesis, and because  $^{40}\text{Ar}/^{39}\text{Ar}$  dating of volcanic tuffs at this  
417 stratigraphic level in the section allow for a constrained age of 33.0 +/- 0.10 to 32.7 +/- 0.03 Ma (Biotite  
418 Tuff and Overlook Tuff, respectively) (Bestland, 1997).



420 **Figure 2. Morphology of three successive paleosols** from the early Oligocene (33 Ma) middle Big Basin Member  
 421 of the John Day Formation in eastern Oregon, USA showing lithology, grain size, horizon designations, and Munsell  
 422 color. The upper paleosol (red with drab green top) is a moderately weathered red Alfisol (Hapludalf in USDA  
 423 Taxonomy); stratigraphically below is a minimally weathered and weakly developed Entisol (Fluvent; tan color); the  
 424 lowest soil (brown color) is an Inceptisol (Andic Eutrochrept, brown color).

425

426 To minimize contamination from modern organic carbon during sampling, all loose surface soil  
 427 and saprolite was removed until the lithified, brick-like unweathered paleosol surface was exposed.  
 428 Below the saprolite of the thin (~30 cm) modern soil, all three paleosols were lithified claystone. Sample  
 429 collection began by trenching with a rock hammer to a ~50 cm depth into (perpendicular to) the lithified  
 430 paleosol sequence. Next, a set of samples were gathered down a vertical transect at approximately 10 cm  
 431 intervals, similar to sampling the horizons of a modern soil, but with rock hammer. Large (~1 kg) lithified  
 432 blocks of claystone were broken out of the outcrop and placed into aluminum foil (ashed at 550° C before  
 433 use) to ensure subsampling for thermal analysis had sufficient volume to expose fresh sample surface  
 434 (e.g., no weathered surfaces were selected for analysis). Small (5-8 g) subsamples were acquired from the  
 435 inside of bulk lithified samples with steel chisels that were previously ashed at 550° C to remove organic  
 436 contaminants. These subsamples were then ground to < 0.02 mm using an agate mortar and pestle (ashed  
 437 at 550° C before use) and stored in glass vials (all ashed at 550° C) prior to thermal analysis and  
 438 radiocarbon dating.

439 No vegetation was present within ~30 m of the sampled paleosol sequence (Figure 2), likely  
440 because the “popcorn” weathering of the smectite-rich modern soil appears to inhibit plant germination  
441 and growth. The Munsell color and qualitative calcareousness of samples were described during  
442 collection. The three paleosols sampled were a red Alfisol (“Luca” pedotype from (Retallack et al.,  
443 2000)), a tan Entisol (“Kskus” pedotype), and a brown Inceptisol (“Ticam” pedotype (Figure 2).

## 444 **2.2 Radiocarbon dating of organic carbon in paleosols**

445 The purpose of radiocarbon ( $^{14}\text{C}$ ) dating was to constrain the age of organic carbon in paleosol  
446 samples. Specifically, radiocarbon dating was used to determine if the organic carbon fraction of  
447 paleosols was entirely endogenous (deposited during soil formation) and had been preserved for millions  
448 of years, or if there had been additions of exogenous organic carbon to paleosols in the last ~45,000 years  
449 (the method-level detection limit for radiocarbon dating techniques). A radiocarbon age of organic carbon  
450 was obtained from four samples, two from the surface and near-surface horizons (A and Bt horizons) of  
451 the stratigraphically highest soil (Alfisol) and two from the surface and near-surface horizons of the  
452 stratigraphically lowest profile (Inceptisol). All samples for radiocarbon dating were acid-washed to  
453 remove inorganic carbonates before radiocarbon dating. For acid washing, ground paleosol samples (~5  
454 g) were treated with approximately 20 mL of 0.1 M HCl at room temperature for 1 hour, then washed  
455 three times with ~30 ml of deionized water and dried at 60° C for 24 hr. Radiocarbon dating of acid-  
456 washed paleosol samples was performed at the W.M. Keck Carbon Cycle Accelerator Mass Spectrometer  
457 at the University of Irvine. The accuracy and precision ( $1\sigma$ ) of this analysis on modern carbon ( $\Delta^{14}\text{C}$   
458 >0‰) was better than 9‰. Laboratory blanks yielded a  $\Delta^{14}\text{C}$  value of -996.2 ‰.

## 459 **2.6 Thermal and evolved gas analysis of paleosol samples**

460 The purpose of this work was to use SAM-EGA-like conditions to characterize bulk gas evolution  
461 and to measure abundance of organic and inorganic carbon in Mars-analog paleosol samples. A Setaram  
462 Labsys Evo differential scanning calorimeter (DSC) / thermal gravimeter (TG) connected to a Pfeiffer  
463 Omnistar QMS was configured to operate similarly to the SAM evolved gas analyzer. The SAM  
464 instrument does not have TG/DSC capabilities, but these components permit a better understanding of  
465 phase transitions and chemical reactions in laboratory experiments. Approximately 50 mg  $\pm$  3 mg of  
466 ground paleosol sample (previously stored in glass vials ashed at 550° C to minimize organic  
467 contamination) were placed in an  $\text{Al}_2\text{O}_3$  sample crucible (also previously ashed at 550° C). The sample  
468 crucible and an identical empty reference crucible were placed in the furnace and then the system was  
469 purged twice with helium gas and set to a pressure of 30 mbar. Helium was chosen as a carrier gas

470 because it is inert and because it used as a carrier gas in the SAM instrument. The crucibles were heated  
471 from approximately 35 °C to 1000 °C at a heating rate of 35°C/min and at a flow rate of 10 sccm.  
472 Volatiles ranging from mass/charge (m/z) 1 - 100 were measured. All analyses were performed in  
473 duplicate.

474 Total organic carbon (TOC) content was determined using a Netzsch TG/DSC coupled to a  
475 Pfeiffer QMS. An Al<sub>2</sub>O<sub>3</sub> sample crucible and an identical reference crucible were placed in the furnace.  
476 The instrument was purged twice with ultra-high purity O<sub>2</sub> and set to a pressure of 1000 mbar prior to  
477 sample analyses to remove any contamination in the system. Oxygen was chosen as a carrier gas because  
478 it encourages complete combustion of all organic and inorganic carbon in samples. The crucibles  
479 containing samples were heated from approximately 35 °C to 1000 °C at a heating rate of 35°C/min and  
480 at a flow rate of 19 ml O<sub>2</sub>/min. A series of three blanks were analyzed before and after each group (n=10)  
481 of samples. A calibration curve for CO<sub>2</sub> was created by analyzing a calcite standard (Iceland sparry calcite  
482 40 µM) at eight sample masses ranging from 0.01 – 4 mg (Table S1). This calibration curve was used to  
483 calculate the amount of CO<sub>2</sub> evolved from each sample, and these values were used to calculate total  
484 carbon in each sample.

485 Thermal techniques including TG-DSC-EGA allow for quantitative estimates of organic and  
486 inorganic carbon without sample pretreatment, in part due to the large differences in thermodynamics and  
487 peak CO<sub>2</sub> release temperatures. By contrast, TOC determinations via elemental analysis involve an acid  
488 pretreatment step to remove carbonates. Paleosol samples were not acid-pretreated for thermal and  
489 evolved gas analyses because some organic carbon can be oxidized during acid-washing (e.g., Apesteguia  
490 et al., 2018). In the present study, carbon was considered organic between 150-550° C and inorganic from  
491 ~700-900° C. Total organic carbon was quantified by deconvolving CO<sub>2</sub> peaks if a carbonate-C peak was  
492 present. This was done by determining the relative percentage of peak area from inorganic carbon-  
493 evolved CO<sub>2</sub> (~700-900° C) then subtracting this value from total carbon-evolved CO<sub>2</sub> peak area to solve  
494 for TOC. All evolved gas plots were background-corrected to account for possible atmospheric  
495 contamination.

## 296 **3. Results/Discussion**

### 497 **3.1 Radiocarbon dating of paleosol organic carbon**

498  
499 Radiocarbon dating of four samples from two different paleosol profiles showed ages between 6265 ±  
500 25 years BP and 14560 ± 170 years BP (Table 1). These samples all showed a distinct signature of  
501 exogenous organic carbon because the samples were not radiocarbon dead (<sup>14</sup>C-free).

**Table 1. Total organic carbon (TOC), total inorganic carbon (TIC) and radiocarbon dating of paleosols examined in this study**

Paleosol	Pedotype ‡	Horizon ¶	Depth in profile (cm)	Total C (wt. %)	TOC (wt. %)†	±σ TOC §	TIC (wt. %)	Expected Age	Δ <sup>14</sup> C <sup>α</sup>	±Δ <sup>14</sup> C	<sup>14</sup> C age (BP) †
Alfisol	Luca	A	4	0.073	0.031	0.0062	0.042	~33 Ma	-	3.85	6265
Alfisol	Luca	A	14	0.094	0.026	0.0097	0.068		543.07		
Alfisol	Luca	Bt <sub>1</sub>	46	0.021	0.018	0.0016	0.003	~33 Ma	-	3.37	14560
Alfisol	Luca	Bt <sub>2</sub>	63	0.067	ND <sup>∪</sup>	-	0.067		838.12		
Alfisol	Luca	C	88	0.033	0.002	0.007	0.031				
Entisol	Kskus	A	100	0.046	0.021	0.0068	0.024				
Entisol	Kskus	C	120	0.036	0.013	0.0037	0.024				
Inceptisol	Ticam	A	125	0.024	0.018	0.007	0.006	~33 Ma	-567.1	1.83	6655
Inceptisol	Ticam	Bw <sub>1</sub>	131	0.027	0.008	0.0013	0.019				
Inceptisol	Ticam	Bw <sub>2</sub>	160	0.020	0.011	0.0023	0.010	~33 Ma	-545.4	1.33	6220
Inceptisol	Ticam	C	175	0.026	0.001	0.0013	0.026				

† Determined by thermal analysis (TG-DSC-EGA) without acid pre-treatment of samples; average of two duplicates. To encourage complete combustion of organic phases in samples, oxygen was used as a carrier gas for determination of total C, TIC and TOC.

‡ Pedotypes (soil orders) are from Retallack et al. 2000

¶ Horizons follow USDA Soil Survey Staff (2014) major horizon designations

∪ ND = No detection; below limit of quantification

§ Standard error for TOC determination from duplicate analysis

<sup>α</sup> Radiocarbon concentrations are given as fractions of the modern standard (fM), Δ<sup>14</sup>C, and conventional radiocarbon age.

502

503           The occurrence of Holocene-age organic matter in paleosol samples was consistent with  
504 diagenetic inputs of organic carbon. There are several possibilities to explain the accumulation of <sup>14</sup>C in  
505 the organic fraction of samples. First, a diagenetic event that occurred between ~6 and ~14 Ka BP could  
506 have delivered exogenous organics into the underlying paleosols, perhaps during exhumation to the  
507 surface and /or leaching of organic acids from surface biota during that time. Cosmogenic exposure dating  
508 such as <sup>10</sup>Be surface exposure dating would provide important evidence to constrain the exhumation  
509 history of the paleosols examined here (Balco et al., 2005; Schiller et al., 2009). However, there was no  
510 sedimentological evidence of exhumation and re-burial of any of the three paleosols at the field site, so  
511 other possibilities to explain the radiocarbon dates were explored.

512           Another possible source of exogenous organic carbon was from precipitation-driven leaching of  
513 dissolved organic carbon from modern biota living in the current weathering zone above the paleosol  
514 outcrop. The fraction of modern carbon (fM) across four samples ranged from 0.469 ± 0.039 to 0.1633 ±  
515 0.034 (Table 1) and was highest in the surface (A horizon, 14 cm) of the Alfisol and lowest in the  
516 subsurface (Bt horizon, 46 cm), suggesting this paleosol contained a mixture of ancient and modern  
517 organic carbon, the latter possibly delivered via precipitation-driven leaching. As such, it is possible that  
518 small amounts of exogenous modern organic carbon from the weathered zone above paleosol outcrops  
519 have mixed with larger amounts of <sup>14</sup>C-free organic carbon endogenous to paleosols. In this way, a  
520 radiocarbon date of ~6-14 Ka BP could represent a mixing of recent/modern organic carbon and ~33 Ma

521 organic carbon. This hypothesis is supported by the erosion rate for the site, which was previously  
522 determined to be  $4.94 \pm 0.05$  mm/yr. (Sweeney et al., 2015). Using this erosion rate, the 20 cm-thick soils  
523 that formed on top of the paleosols are only about 40 years old and could have leached modern organics  
524 into the underlying paleosols during this time.

525         There was also a weak relationship between the radiocarbon age and the depth into the outcrop  
526 where the sample was collected (Table 1). Younger radiocarbon dates were observed in shallower  
527 samples taken closer to the modern weathering zone. However, a decrease in  $^{14}\text{C}$  content with depth is  
528 commonly observed in modern soils because subsurface horizons preferentially accumulate older,  
529 refractory organic carbon primarily via sorption to surfaces of minerals and amorphous phases (Lawrence  
530 et al., 2021). Across four paleosol samples in this work, the radiocarbon age generally increased with  
531 depth, suggesting there may be age-depth relationship for samples (Table 1), but this result should be  
532 interpreted with caution because only four samples were dated in this work, and because age-depth trends  
533 are routinely observed in modern soils (Ewing et al., 2008). In any case, there may be a sampling depth  
534 (i.e., > 1 meter) that significantly reduces or eliminates exogenous carbon additions to paleosols. These  
535 demonstrate that radiocarbon dating can be a useful technique for constraining the age of organic carbon  
536 in ancient terrestrial surface environments.

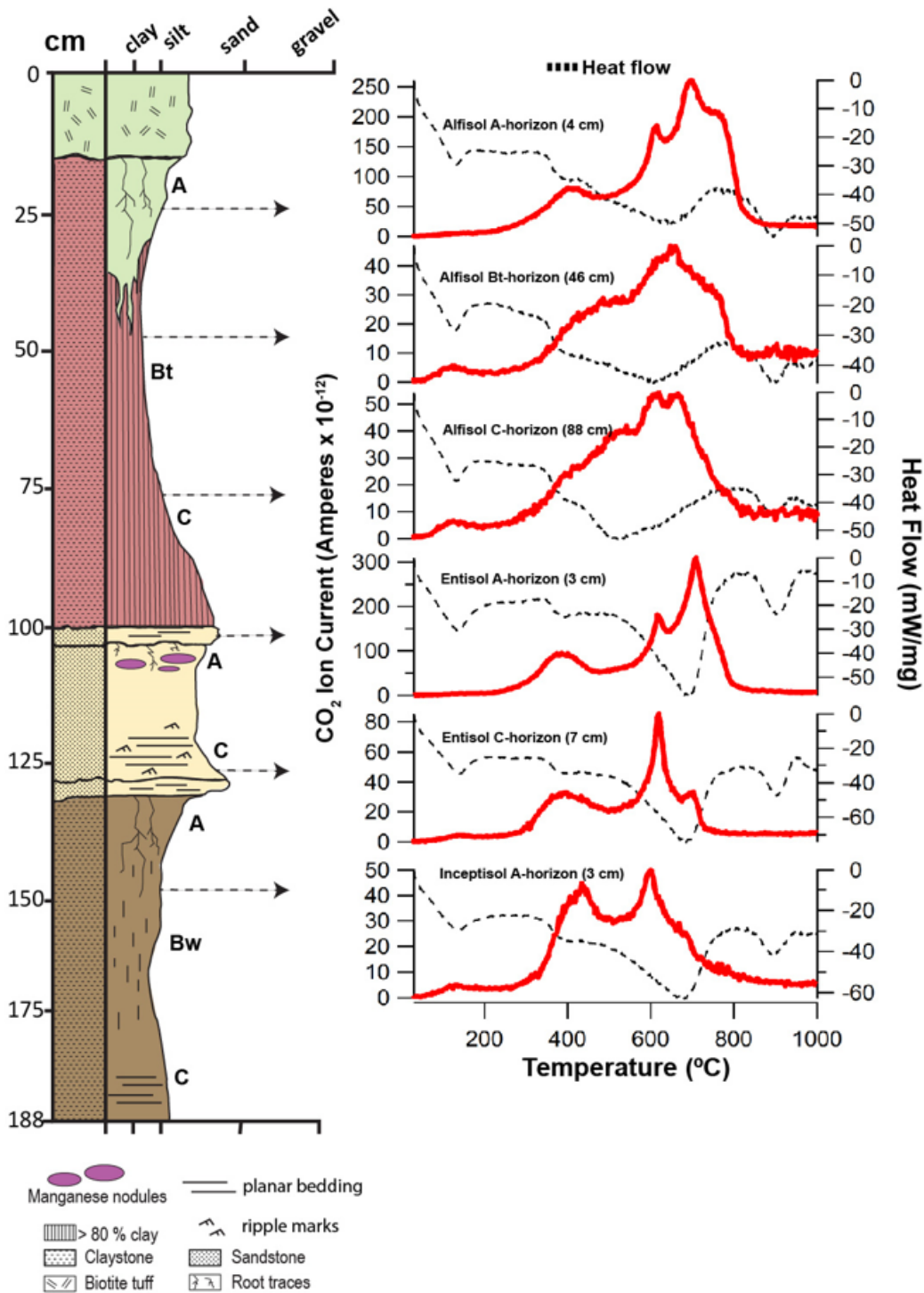
537

## 538 **3.2 Thermal and Evolved Gas Analysis**

### 539 **3.2.1 CO<sub>2</sub> and CO evolutions**

540         When subject to thermal and evolved gas analysis, all samples evolved CO<sub>2</sub> at temperatures  
541 ranging from ~150 – 800° C and had two distinctive CO<sub>2</sub> peaks (Figure 3). A broad low temperature ~200  
542 - 500° C peak was followed by a sharp high-temperature peak at ~650-750° C which was observed in all  
543 samples. CO<sub>2</sub> evolved at 150-500° C is primarily from organic carbon decomposition (Sutter et al., 2017;  
544 Apesteguia et al., 2018) but also possible are contributions are from CO<sub>2</sub> inclusions in minerals or  
545 amorphous phases, or from adsorbed atmospheric CO<sub>2</sub> (Ming et al., 2014). The organic C contributing to  
546 evolved CO<sub>2</sub> is most likely from simple organic compounds (<350° C) or refractory macromolecular  
547 organic compounds (300-600° C) (Eigenbrode et al., 2018).

548



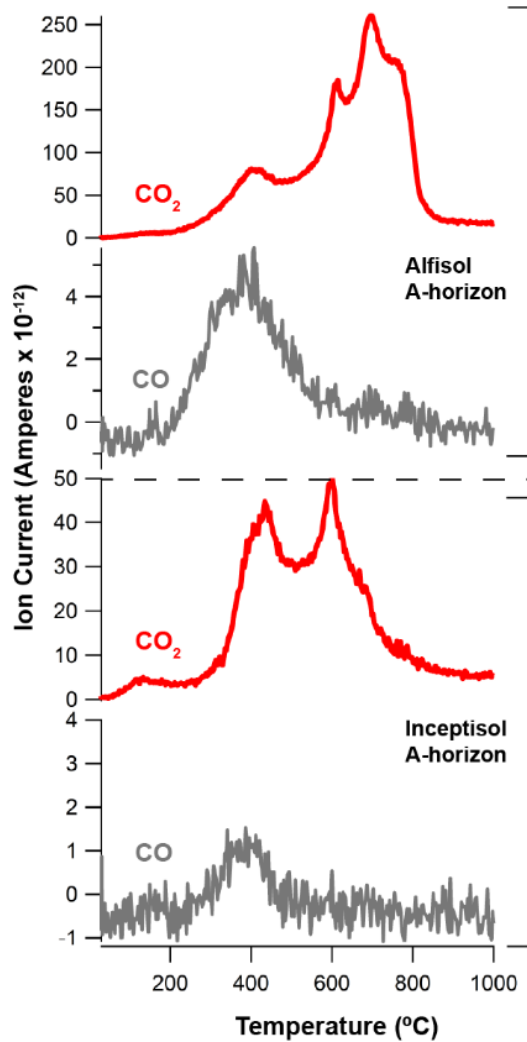
550 **Figure 3. Evolutions of CO<sub>2</sub> (red traces) and heat flow (dashed traces) from early Oligocene (33 Ma) Al/Fe**  
 551 **smectite-rich paleosols from the John Day Fossil Beds National Monument, Oregon. Red trace is CO<sub>2</sub> (m/z 44)**  
 552 **and dashed trace is heat flow from differential scanning calorimetry (DSC). Helium was used as a carrier gas for all**  
 553 **analyses.**  
 554

555 The endothermic thermal decomposition of Ca carbonate was a probable source of CO<sub>2</sub> release  
556 from approximately 550 – 800° C (Cannon et al., 2012; Sutter et al., 2012). High temperature (> 650° C)  
557 CO<sub>2</sub> evolutions generally exceeded the low temperature (150-550° C) CO<sub>2</sub> evolutions in peak area across  
558 all samples, though both high temperature and low temperature CO<sub>2</sub> evolutions were on the same order of  
559 magnitude. Total inorganic carbon (TIC) values varied from 0.006 to 0.068 wt. % (Table 1) and the ratio  
560 of inorganic carbon to total carbon ranged from 0.14 to 1, consistent with variable mixtures of Ca  
561 carbonate and organic carbon in each sample. There are well-defined Ca carbonate endotherms in the heat  
562 flow data from the Entisol and Inceptisol, but this trend was not so well-defined in the Alfisol (Figure 3)  
563 and there also appears to be “doublet” high-temperature CO<sub>2</sub> peaks for the Entisol, suggesting a  
564 combination of Ca-carbonate and perhaps dolomite or ankerite, though these phases were not previously  
565 observed with XRD (Table S6). DSC-EGA analysis of modern soils containing various amounts of calcite  
566 have a similar sharp endothermic CO<sub>2</sub> peak release temperature at ~700° C which was attributed to the  
567 thermal decomposition of Ca carbonate (Apesteguia et al., 2018). An additional ~900° C endotherm  
568 observed in all samples was unrelated to carbonate decomposition and instead was attributed to thermal  
569 decomposition of sulfate minerals such as jarosite, which was previously detected in trace amounts with  
570 x-ray diffraction (Table S6). Interestingly, Ca-carbonate was not previously identified from x-ray  
571 diffraction patterns (Table S6 and Figure S3), and thus it is likely that these samples contain inorganic  
572 carbonate below detection limit of XRD (~1 wt. %), but not SAM-EGA (0.01 wt. %). This agrees with  
573 estimated abundances of TIC which were below 1 wt. % (Table 1) and demonstrates the ability of SAM-  
574 EGA-like analyses to detect trace amounts of inorganic carbon in complex pedogenic mineral matrices.

575 Other sources of high temperature CO<sub>2</sub> release could have result from the decarboxylation of  
576 organic compounds in refractory or thermally mature organic matter which occur over a broad range of  
577 temperatures (150 - 800° C). Previous investigation showed no coalification of organic matter or  
578 development of secondary porosity in any paleosols from the Painted Hills, which were buried by an  
579 estimated 1.5 - 2 km of overburden (Retallack et al., 2000; Horgan, 2016), suggesting paleosol samples  
580 here contain refractory but not thermally mature organic compounds.

581  
582 All samples evolved CO with a peak release temperature of ~400° C (Figure 4). The sample with  
583 the highest total organic carbon detected (~0.03 wt. %, surface horizon of Alfisol) evolved a CO<sub>2</sub> release  
584 peak at ~400° C that co-occurred with the release of CO. This trend of coevolved CO and CO<sub>2</sub> at ~400° C  
585 was observed across all paleosol samples. Evolution of CO was consistent with incomplete combustion of  
586 organics and/ or the presence of oxygen-bearing organics (Sutter et al., 2017). The co-occurrence of CO  
587 and CO<sub>2</sub> was not observed at high (~700° C) temperatures (Figure 4) because the thermal decomposition

588 of Ca carbonate does not produce CO. Thus, evolved CO detections near 400° C were consistent with the  
 589 decomposition of organic compounds.

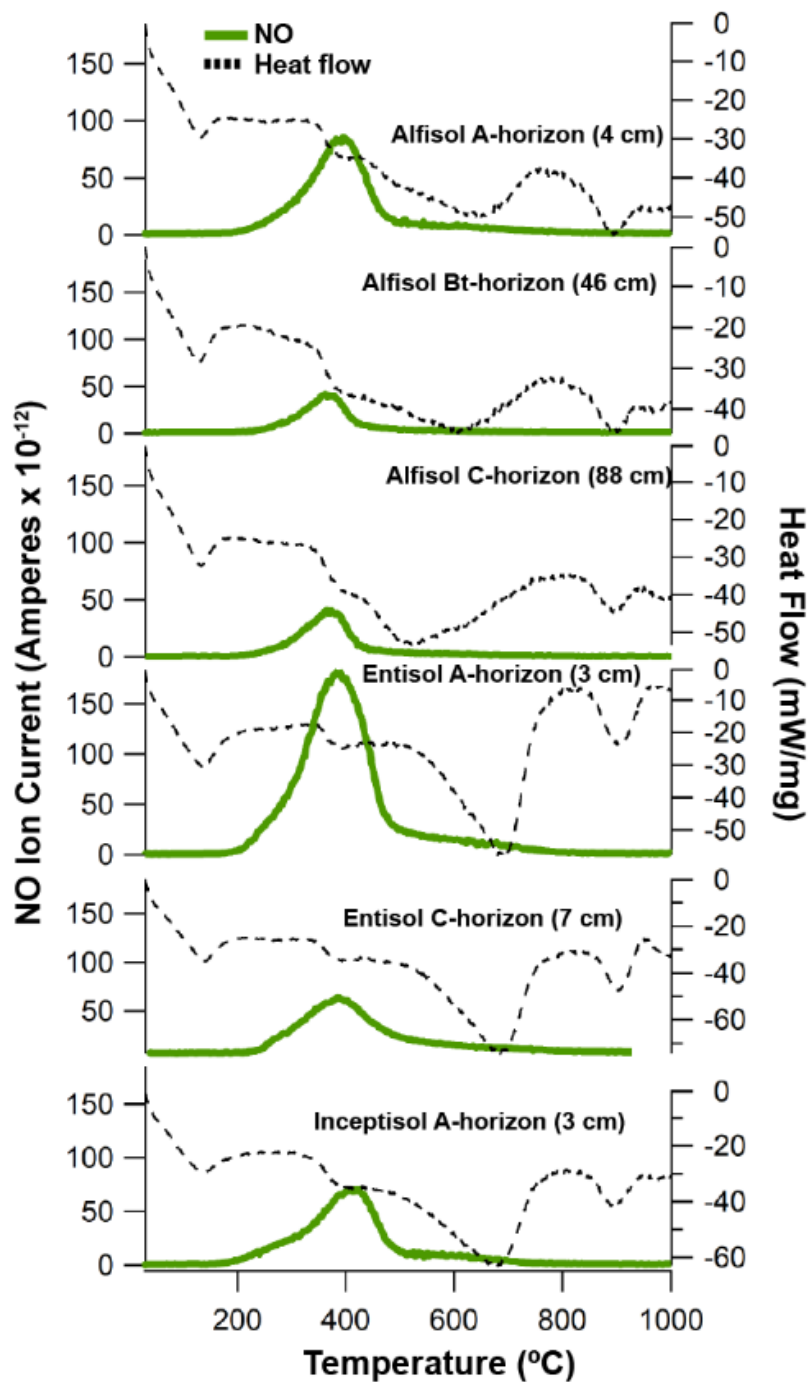


591  
 592 **Figure 4. CO<sub>2</sub> (red trace) and CO (m/z 28) (grey trace) evolutions from the surface horizons of paleosols at**  
 593 **the John Day Fossil Beds National Monument, Oregon.** Top panel is surface (4 cm) horizon of an Alfisol; bottom  
 594 panel is surface (3 cm) horizon of an Inceptisol.  
 595

596 **3.2.2 NO evolutions**

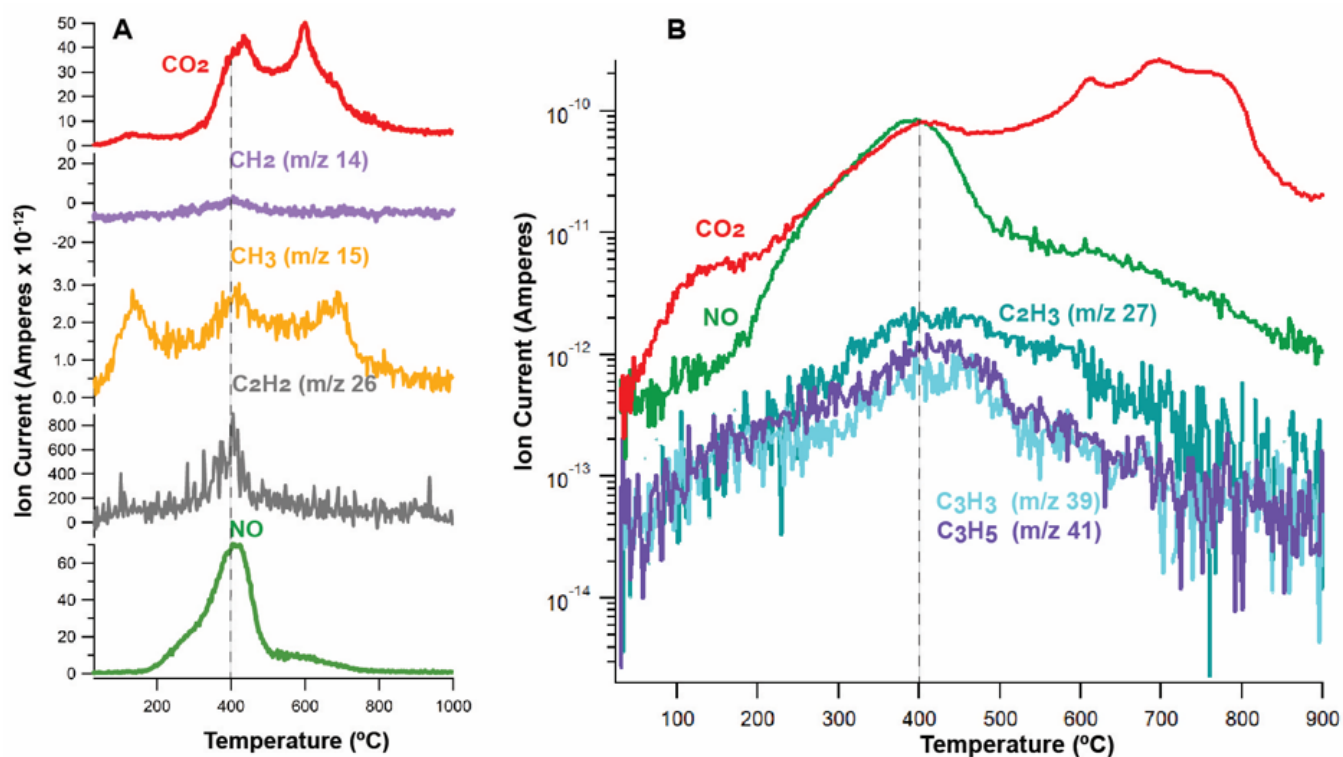
597 Nitric oxide (NO; m/z 30) was detected in all paleosol samples (Figure 5) and was consistent with  
 598 the oxidation of nitrogen-bearing organics. In the sample with the greatest amount of organic carbon  
 599 (Alfisol A-horizon), evolutions of NO start at ~300° C and show peak release temperature of ~ 400° C  
 600 and a shoulder at ~ 600° C (Figure 5). Additionally, organic fragments observed in this sample included  
 601 CH<sub>2</sub> (m/z 14), CH<sub>3</sub> (m/z 15), and C<sub>2</sub>H<sub>2</sub> (m/z 26) (Figure 6). Evolutions of NO were simultaneous with

602 evolutions of these organic fragments at  $\sim 400^\circ\text{C}$ , suggesting the oxidation of a nitrogen-bearing organic  
 603 compound was a significant contributor to evolved NO (Stern et al., 2015).



605 **Figure 5. Evolutions of nitric oxide (NO) from paleosols at the John Day Fossil Beds National Monument,**  
 606 **Oregon.** Green trace is NO ( $m/z$  30) and dashed trace is heat flow from differential scanning calorimetry (DSC).  
 607

608 The thermal decomposition of nitrates can also release NO, though at elevated temperatures (>  
 609 500° C) relative to nitrogenated organics (Stern et al., 2015), and therefore the release peak temperature of  
 610 NO release can constrain the source of NO. For example Alkali (Na, K) and alkaline earth (Mg, Ca) metal  
 611 nitrates decompose to NO at temperatures > 560° C (Stern et al., 2015). In laboratory experiments under  
 612 SAM-like conditions, Fe(NO<sub>3</sub>)<sub>3</sub> begins to decompose to NO at < 200° C and exhibits two distinct  
 613 releases of NO at ~300 and ~450° C, which has been attributed to dehydration and hydrolysis of  
 614 Fe(NO<sub>3</sub>)<sub>3</sub>, respectively (Stern et al., 2015). Instead, NO release in paleosol samples began at ~250° C and  
 615 exhibited a single peak at ~400° C across all samples (Figure 5), unlike the dual high-temperature NO  
 616 peaks from decomposition of Fe(NO<sub>3</sub>)<sub>3</sub>. The simultaneous evolution of NO, CO<sub>2</sub>, and organic fragments  
 617 in paleosol samples analyzed here (Figure 6) are an additional line of evidence suggesting NO releases  
 618 could have resulted from oxidation and/or decarboxylation of nitrogen-bearing organic compounds.



620 **Figure 6. Simultaneous evolutions of CO<sub>2</sub>, NO (m/z 30) and organic fragments in paleosol surface horizons.**  
 621 (A) Evolutions of CO<sub>2</sub>, NO (m/z 30), and organic fragments (m/z 14, 15, 26) from the surface horizon of the  
 622 Inceptisol (3 cm). (B) Semi-log scale plot of CO<sub>2</sub>, NO and additional organic fragments (m/z 27, 39, 41) from the  
 623 surface horizon (4 cm) of the Alfisol

624

625

626 One possible source of nitrogen-bearing organic carbon compounds is pyrogenic carbon (char) in  
 627 paleosol samples that formed as a result of wildfires across the original soil landscape (Kurth et al., 2006).  
 628 Nitrogen-bearing organic compounds such as nitriles, pyridine and pyrrole-derive compounds have been

629 observed with pyrolysis GC/MS in modern fire-affected soils (De la Rosa et al., 2008). These modern  
630 soils were also observed to have a broad  $\sim 400^\circ\text{C}$  peak release temperature of NO ( $m/z$  30) during TG-  
631 DSC-EGA, suggesting that pyrogenic carbon may be the source of low-temperature NO release in soils.  
632 However, the fire history of paleosols in the present study has not yet been investigated. Although it is  
633 impossible to determine the original inputs of nitrogen-bearing organics in paleosols, nitrogen may have  
634 been incorporated into increasingly stable organic matter as a consequence of forest fires, and may persist  
635 in paleosols today as char. Previous authors have reported the occurrence of preserved char in paleosols  
636 of late Permian (Miller et al., 1996) and late Jurassic age (Matthewman et al., 2012) paleosols,  
637 respectively, so it is plausible that nitrogen-bearing char may be responsible for the overlapping  $\sim 400^\circ\text{C}$   
638 NO and CO<sub>2</sub> peaks observed here.

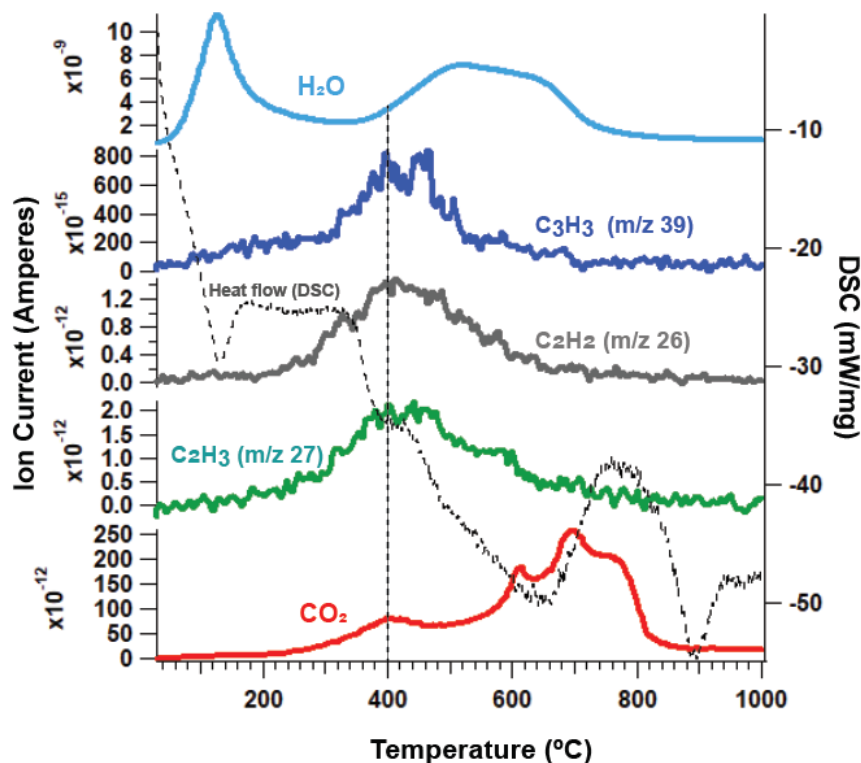
639

### 640 **3.3 Possible mechanisms of organic carbon preservation in paleosols**

641 We observed evolutions of volatile gases from clay-rich paleosols that may have resulted from  
642 the preservation of organic carbon over geological time scales. The fragmentation of organic molecules  
643 during pyrolysis EGA provides limited constraints on the types of molecules present, but it can help  
644 determine if there are any associations between minerals and organic molecules. These associations can  
645 include physical occlusion, chemisorption and/or adsorption to mineral surfaces, or intercalation in clay  
646 minerals (Kleber et al., 2005, 2021; Schmidt et al., 2011; François et al., 2015). A strong correlation  
647 between the peak release temperature of organic fragments and the release of H<sub>2</sub>O or other volatiles  
648 would suggest that organic matter could have been associated with minerals.

649 One line of evidence that organic molecules may have persisted in association with clay minerals  
650 is co-occurring evolutions of organic fragments, CO<sub>2</sub>, and water releases from clay dehydroxylation. Al-  
651 smectite in the surface horizon of the Alfisol began dehydroxylating at  $\sim 400^\circ\text{C}$  (broad H<sub>2</sub>O peak) which  
652 co-occurred with evolutions of CO<sub>2</sub> and organic fragments (Figure 7). This sample had the highest TOC  
653 ( $\sim 0.03$  wt. %, Table 1), a radiocarbon date of  $\sim 6300$  years BP and a phyllosilicate content of  $\sim 85$  wt. %  
654 (Table S1). The high clay mineral content could be related to the abundance of organic carbon in this  
655 sample. Many of the deeper samples had higher temperatures of clay dehydroxylation due to differences  
656 in clay mineralogy and/or abundance, such as the Entisol and Alfisol (Figure S1). These samples were  
657 depleted in organic carbon (Table 1) relative to the Al smectite-rich surface horizon of the Alfisol.  
658 Additional investigations such as microscale imaging (e.g., transmission electron microscopy) and  
659 methods to characterize the bonding environments between minerals and organics in paleosols are needed  
660 to support this interpretation.

661

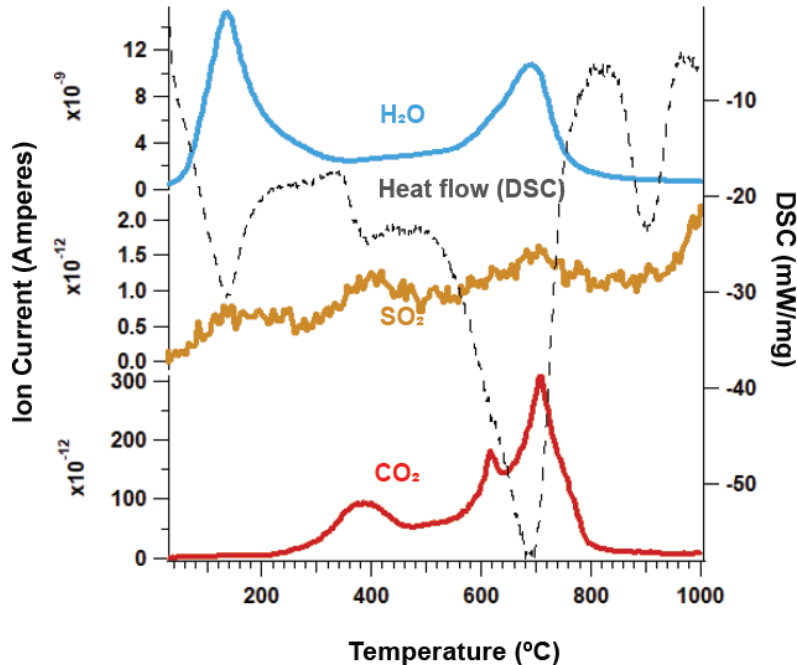


663 **Figure 7. Evolutions of CO<sub>2</sub>, organic fragments, and H<sub>2</sub>O from the surface horizon of the Alfisol (4 cm).** Co-  
 664 occurring releases of CO<sub>2</sub> and organic fragments at the onset of Al-smectite dehydroxylation (H<sub>2</sub>O release at ~400°  
 665 C, vertical dotted line) suggest organic molecules may have been associated with clay minerals. Dashed trace is heat  
 666 flow from differential scanning calorimetry (DSC).

667  
 668 It is important to note that there are many competing factors that control the preservation and  
 669 degradation of organic carbon in terrestrial environments. Minerals themselves may facilitate oxidation of  
 670 organic carbon compounds (Kleber et al., 2021), as is the case with certain Mn-bearing minerals (Reardon  
 671 et al., 2016). Paleosols examined here contained between ~70-90 wt. % smectite, primarily as mixtures of  
 672 montmorillonite and nontronite (Tables S4 and S6). Possible mechanisms of organic carbon preservation  
 673 include the formation of organo-mineral complexes, and/or the formation of microaggregates which may  
 674 have increased the biochemical stability of organic molecules, as observed in modern soils (Plante et al.,  
 675 2011) and Quaternary paleosols (Marin-Spiotta et al., 2014). Smectite clay minerals in particular preserve  
 676 organic molecules due to their high specific surface area, negatively charged interlayers, and cations  
 677 which inhibit water flow, thus making them favorable locations for the preservation of organic carbon  
 678 over millions or possibly billions of years (Bishop et al., 2013; Noe Dobrea et al., 2016; Szopa et al.,  
 679 2020).

680 Interactions with sulfur can also aid in the preservation of organic molecules in soils and  
 681 sediments over geological time scales (Matthewman et al., 2012; François et al., 2015; Eigenbrode et al.,  
 682 2018; Alekseeva et al., 2019). The incorporation of organic C into the crystal lattice of sulfate minerals

683 can increase thermodynamic stability and therefore increase the temperature of organic carbon  
 684 decomposition during EGA (François et al., 2015). Minor detections of jarosite and gypsum in XRD  
 685 patterns (< 5 wt. %) were observed, and these minerals could have also contributed to the preservation of  
 686 organics (Tables S5 and S6). Minor SO<sub>2</sub> evolutions at ~800° C across all samples (Figure S1) were  
 687 consistent with the decomposition of sulfate minerals. A single sample (Entisol 7 cm) had a low-  
 688 temperature SO<sub>2</sub> peak that co-occurred with the CO<sub>2</sub> release at ~400° C (Figure 8).



690 **Figure 8. Evolutions of H<sub>2</sub>O (blue trace), SO<sub>2</sub> (yellow trace), CO<sub>2</sub> (red trace), and heat flow (dashed trace)**  
 691 **from the surface horizon of the Entisol (3 cm).** DSC – differential scanning calorimetry (heat flow), H<sub>2</sub>O – m/z  
 692 18, SO<sub>2</sub> – m/z 64, CO<sub>2</sub> – m/z 44.

693

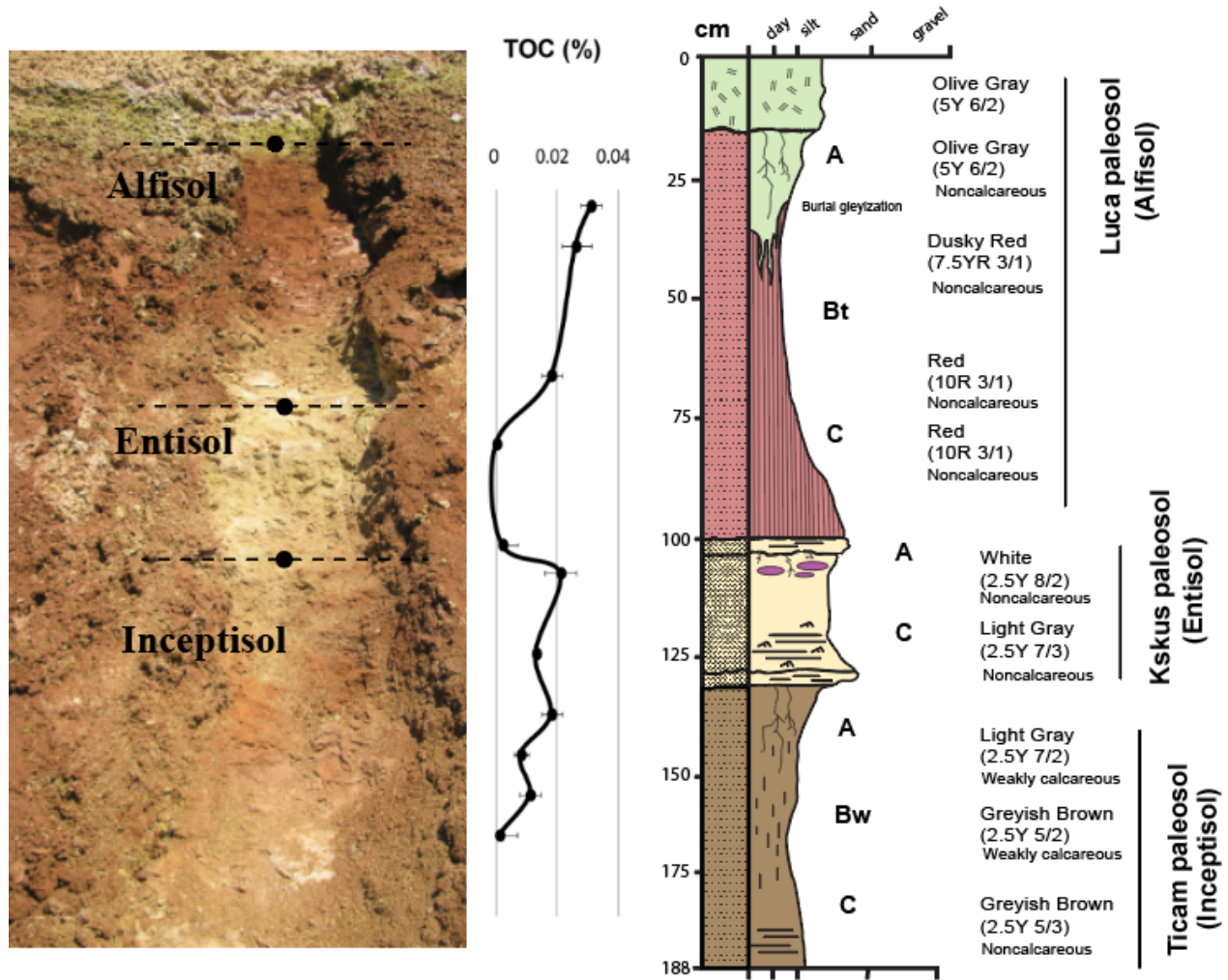
694 Trace amounts of Mg sulfates in the Alfisol could account for minor SO<sub>2</sub> releases > 700° C  
 695 including the ~790° C SO<sub>2</sub> peaks (François et al., 2015; Mcadam et al., 2020a). At higher temperatures,  
 696 all soils showed a major release of SO<sub>2</sub> beginning at 900° C which co-occurred with an endotherm, both  
 697 of which are consistent with the thermal decomposition of crystalline sulfates (Ming et al., 2014; François  
 698 et al., 2015). Since the samples were only heated to ~1000° C for this work, the maximum peak height of  
 699 this release cannot be ascertained. Across most samples, peak SO<sub>2</sub> release temperatures generally did not  
 700 co-occur with low-temperature (~400° C) CO<sub>2</sub> evolutions across the rest of the samples (Figure S1), so it  
 701 is unlikely that sulfate minerals played a significant role in organic preservation in samples examined  
 702 here.

703

704

705 **3.4 Enrichment of organic carbon in surface layers of paleosols**

706 The near-surface horizons of all paleosols examined here had greater amounts of total organic  
 707 carbon (TOC) relative to deeper horizons (Figure 9, Table 1). The highest amounts of CO<sub>2</sub> released from  
 708 decomposition of organic carbon (150-500° C) were in the near surface (A) horizons of all three paleosol  
 709 types while subsurface layers of paleosols generally had lower quantities of evolved CO<sub>2</sub> from organic  
 710 carbon (Figure 3, Table 1). The A horizon of the Alfisol had TOC of 0.031 ± 0.006 wt. % and  
 711 progressively decreased to 0.002 ± 0.007 wt. % in the C horizon.



713 **Figure 9. Trends of organic carbon enrichment in the near-surface horizons of three paleosols** from the early  
 714 Oligocene (33 Ma) middle Big Basin Member of the John Day Formation in eastern Oregon, USA. The surface (A)  
 715 horizons of all three profiles had significantly ( $P > 0.05$ ) higher total organic carbon (TOC) content relative to  
 716 subsurface horizons (Bt, Bw and C horizons, respectively). Average TOC content of samples ( $n=2$ ) was determined  
 717 by thermal and evolved gas analysis (oxygen as a carrier gas).  
 718

719 Samples from the A-horizon of the Alfisol had been affected by burial gleization. Burial  
 720 gleization is an early diagenetic process in paleosols which involves the reduction of Fe<sup>3+</sup> to Fe<sup>2+</sup> by

721 anaerobic microbes as a result of rapid burial (PiPujol and Buurman, 1994; Retallack, 2019). This is also  
722 thought to promote anaerobic decay of organic matter (Retallack, 2019), even in soils that originally  
723 formed under oxidizing conditions before burial. Typical burial gleization is closed system alteration,  
724 without depletion of total iron, and is usually limited to the surface horizons where organic matter is most  
725 concentrated. The surface horizon of the Alfisol examined in this work showed classic evidence of burial  
726 gleization with drab-colored mottles and tubular features predominantly in the A-horizon with minor  
727 radiation downward into the subsurface (Bt) horizon (Figure 9). Rapid emplacement of a biotite-bearing  
728 tuff on the paleosurface of the Alfisol may have led to gleization. Similar trends of near-surface TOC  
729 enrichment were noted in the Entisol and Alfisol (Table 1), but these samples lacked chemical  
730 ( $\text{FeO}/\text{Fe}_2\text{O}_3 > 0$ ) and morphological evidence (drab green color) of burial gleization (Table S3). Previous  
731 work on terrestrial paleosols has shown positive and significant correlations between  $\text{Fe}^{2+}$  and TOC  
732 (Broz, 2020). This supports the interpretation that burial gleization, which increases  $\text{Fe}^{2+}$  in bulk samples,  
733 may have been associated with the preservation of organic carbon in the surface horizon of the Alfisol.  
734

735         Organic carbon from organisms living in surface horizons of soils may have been preserved upon  
736 rapid burial of the paleosurface, and therefore the trend of surface enrichment may represent the  
737 preservation of endogenous organic carbon. Alternatively, diagenetic additions of carbon may have  
738 accumulated in near-surface layers of each profile. Major losses of endogenous organic carbon from early  
739 diagenetic burial decomposition of organic matter are common in paleosols that originally formed under  
740 oxidizing conditions such as those examined here (Retallack, 2019). Despite diagenetic additions and  
741 losses of organic carbon, the trend of surface enrichment of organic carbon remains apparent, even in  
742 soils that formed under strongly oxidizing conditions prior to burial. These results are consistent with  
743 other studies of paleosols where surface enrichment of organic carbon was observed (Rye and Holland,  
744 2000; Watanabe et al., 2004; Liivamägi et al., 2018; Liu et al., 2020). However, it is possible that late  
745 diagenetic inputs of organics caused this enrichment, for example, by preferential flow and accumulation  
746 in the paleosurface of each profile. Considering the Holocene radiocarbon dates for these ~33 Ma  
747 paleosols (Table 1), results from this work cannot definitively rule out diagenesis as a mechanism for  
748 surface enrichment, though it is unlikely that early and/or late diagenetic additions of organic carbon  
749 would have preferentially accumulated in the near-surface horizons of these buried soils.  
750

### 751 **3.5 Implications for Mars**

752         Recent work has considered putative paleosols on Mars as potential high priority environments  
753 for *in-situ* biosignature investigation (Hays et al., 2017) and Mars Sample Return (Bishop et al., 2018a).  
754 This is because the composition and properties of paleosols preserve evidence of paleoclimate, aqueous

755 conditions, and life (Bishop et al., 2018a). A major finding of this study is that near-surface horizons of  
756 terrestrial paleosols appear to be a favorable location for SAM-EGA detection of organic carbon. Like  
757 modern soils, the surface layers of Mars-analog paleosols examined here show evidence of surface  
758 enrichment of organic carbon. Although the early diagenetic process of burial decomposition of organic  
759 matter has likely reduced the organic carbon content of these ancient soils by at least two orders of  
760 magnitude relative to modern soils (Broz, 2020), the enrichment of organic carbon in surface horizons  
761 (~0.03 wt. %) and subsequent depletion in deeper layers (<0.01 wt. %) was readily observable with  
762 SAM-EGA analog instrument.

763 Results from this study also have implications for interpreting the chemical and isotopic  
764 biosignature preservation potential of Al and Fe smectite-bearing weathering profiles on Mars. However,  
765 as discussed earlier, there are critical limitations to using terrestrial paleosols as analogs to interpret the  
766 organic preservation potential of paleosols on Mars, such as major differences in the types and properties  
767 of organic molecules deposited during soil formation. Irrevocable differences between Earth and Mars,  
768 including climate and a complex terrestrial biosphere, preclude direct comparisons. In any case,  
769 observations of refractory organic compounds that persist in terrestrial paleosols with Mars-like  
770 mineralogy provides a reference frame for interpreting future observations of putative weathering profiles  
771 on Mars. It is possible that clay minerals and/or amorphous phases in martian weathering profiles impart a  
772 similar control on the fate of organic carbon.

773 Results from this work also provide an initial framework for investigation and sampling of  
774 martian weathering profiles should they be encountered by current or future landed missions. Future *in-*  
775 *situ* analysis of putative weathering profiles should begin at the surface and sample down the into the  
776 unaltered protolith. However, if the entire profile is not accessible for investigation (e.g., outcrop is at a  
777 topographic position inaccessible to the rover), the near-surface horizons of the profile, just below the  
778 uppermost burial layer, should be considered the highest priority target for remote sensing, contact  
779 science, and collection of a drilled sample for sample return to Earth.

780

## 781 **Conclusions**

782 The objectives of this study were a) to determine whether the organic carbon content of ~30-  
783 million-year-old paleosols can be detected with a thermal and evolved gas analyzer configured to operate  
784 like the SAM-EGA instrument onboard *Curiosity* Mars rover, and b) use radiocarbon ( $^{14}\text{C}$ ) dating to  
785 constrain the age of organic carbon in bulk paleosol samples. Radiocarbon dating of organic carbon in  
786 four paleosol samples revealed the presence of recent and/or modern exogenous organic carbon. Samples  
787 from 0 - 20 cm were dated to ~6,200 years BP and had a fraction modern (fM) value of ~0.4, while a

788 single deeper sample collected from 43 cm had a radiocarbon age of ~14,600 years BP and ~0.16 fM. The  
789 presence of radiocarbon in paleosols could have resulted from the diagenetic addition of small amounts of  
790 modern (< 1 Ka) organic carbon which mixed with <sup>14</sup>C-free endogenous organic carbon. Alternatively, a  
791 diagenetic event between 6-14 Ka could have introduced exogenous organics, possibly through  
792 groundwater alteration and/or precipitation-driven leaching of dissolved organic carbon. There may be a  
793 sampling depth (e.g., > 1 meter into the outcrop) which decreases or eliminates organic additions from  
794 exogenous sources. It is possible, however, that diagenesis has pervasively introduced exogenous organic  
795 carbon to deeper samples. Holocene-age radiocarbon dates supported the hypothesis that paleosols from  
796 the site contain exogenous organic carbon. These results highlight major challenges for determining the  
797 source(s) and age of organic matter in terrestrial paleosols. Radiocarbon dating should be used in future  
798 analog studies to help distinguish diagenetic organic inputs from original endogenous inputs.

799 SAM-EGA-like characterization of paleosols showed evolutions of CO, NO, CO<sub>2</sub>, and organic  
800 fragments. Coevolutions of CO<sub>2</sub> and organic fragments at ~400° C suggested the presence of refractory  
801 organic carbon. However, like other oxidized terrestrial paleosols of Cenozoic age and older, only trace  
802 amounts (<0.1 wt. %) of organic carbon was detected, which most likely was a result of diagenetic  
803 decomposition of organic matter over geological time scales. Many samples examined in this work  
804 typically contained very low amounts (~0.01 wt. %) of organic carbon, but these low values were  
805 nevertheless detectable by SAM-like evolved gas analysis of bulk samples. These results suggest the  
806 organic fraction of potential martian weathering profiles may be detectable with evolved gas analysis,  
807 even if organic concentrations are low.

808 A major result of this work was that organic carbon was concentrated in near-surface horizons of  
809 paleosols while deeper horizons were depleted in organic carbon. Like modern soils, these ancient soils  
810 were enriched in organic carbon in near-surface horizons, and it appears that this trend persisted in these  
811 samples despite burial decomposition of organic carbon over geological time scales. Alternatively,  
812 diagenesis could have pervasively introduced exogenous organic carbon, but it is unlikely such organic  
813 contamination would preferentially accumulate in the surface layers of each successive buried soil profile.  
814 Surface enrichment of organic carbon in possible weathering profiles on Mars may therefore constitute a  
815 putative chemical biosignature. This work demonstrates that analytical techniques similar to SAM-EGA  
816 can detect trace amounts of organic carbon in complex pedogenic mineral matrices. The search for past  
817 life on ancient land surfaces of Mars should include targeting Martian weathering profiles for *in-situ*  
818 biosignature investigation and Mars Sample Return.

819

## 820 **Additional Information**

821

822 **Acknowledgements**

823 This work was performed on the ancestral homelands of the Numu, Cayuse, Umatilla, Walla Walla, and  
824 Confederated Tribes of the Warm Springs who were present before western settlement. Many thanks to  
825 Elizabeth Rampe and Paul Niles for the opportunity to work on this project and for providing research  
826 direction during a summer internship. Megan Barrington and Barry Hughes assisted with fieldwork and  
827 entertained thoughtful discussion. Angela Olsen, Marshall Styczinski, Paul Regensberger and Joe  
828 Caggiano reviewed early versions of the manuscript. Funding to A.P.B. from the National Science  
829 Foundation, Geological Society of America, The Clay Minerals Society, The Society of Sedimentary  
830 Geology, and the Central Oregon Geoscience Society aided in the completion of this project.

831

832 **Author Contribution Statement**

833 A.P.B and J.V.C designed the study, performed all laboratory analyses and drafted the manuscript. J.V.C,  
834 D.W.M, P.D.A, and B.S contributed to data analysis and interpretation. B.H.H identified similarities  
835 between Mars and Oregon paleosols and assisted with fieldwork and data interpretation. L.C.R.S  
836 provided radiocarbon analyses and interpreted the data. J.V.C, P.D.A, B.S, D.W.M, and L.C.R.S  
837 supervised the project. A.P.B drafted all figures. All authors contributed to the manuscript.

838

839 **Author Disclosure Statement**

840 No competing financial interests exist.

841 **Data Availability Statement**

842 All data supporting the conclusions can be found within the article and in the following repository:  
843 Mendeley Data, V4, DOI: 10.17632/bkvcff9dw8.1. All raw data to reproduce EGA traces are included in  
844 the Mendeley repository (<https://data.mendeley.com/datasets/bkvcff9dw8/1>).

845

846

847 **4 References**

848 Alekseeva, T. V, Zolotareva, B.N., and Kolyagin, Y.G., 2019, Nonhydrolyzable Part of Soil  
849 Organic Matter in Buried and Modern Soils: *Eurasian Soil Science*, v. 52, p. 632–643,  
850 doi:10.1134/S1064229319060024.

851 Amundson, R., 2018, Meteoric water alteration of soil and landscapes at Meridiani Planum,  
852 Mars: *Earth and Planetary Science Letters*, v. 488, p. 155–167,  
853 doi:10.1016/j.epsl.2018.02.012.

854 Apesteguia, M., Plante, A.F., and Virto, I., 2018, Methods assessment for organic and inorganic  
855 carbon quantification in calcareous soils of the Mediterranean region: *Geoderma Regional*,  
856 v. 12, p. 39–48, doi:10.1016/j.geodrs.2017.12.001.

- 857 Archer, P. et al., 2014, Abundances and implications of volatile-bearing species from evolved  
858 gas analysis of the Rocknest aeolian deposit, Gale Crater, Mars: *Journal of Geophysical*  
859 *Research : Planets*, p. 237–254, doi:10.1002/2013JE004493.Received.
- 860 Balco, G., Stone, J.O.H., and Mason, J.A., 2005, Numerical ages for Plio-Pleistocene glacial  
861 sediment sequences by Al / 10 Be dating of quartz in buried paleosols: *Earth and Planetary*  
862 *Science Letters*, v. 232, p. 179–191, doi:10.1016/j.epsl.2004.12.013.
- 863 Beaty, D.W., Grady, M.M., Mcsween, H.Y., Sefton-Nash, E., Carrier, B., Altieri, F., and Al., E.,  
864 2019, The potential science and engineering value of samples delivered to Earth by Mars  
865 sample return: *Meteoritics & Planetary Science*, v. 671, p. 667–671,  
866 doi:10.1111/maps.13232.
- 867 Bestland, E., 1997, Alluvial Terraces and Paleosols As Indicators Of Early Oligocene Climate  
868 Change (John-Day Formation, Oregon): *Journal Of Sedimentary Research*, v. 67, p. 840–  
869 855, doi:10.1306/D4268653-2B26-11D7-8648000102C1865D.
- 870 Bestland, E.A., 2002, Fossil Andisols identified with mass-balance geochemistry (Oligocene  
871 John Day Formation, Oregon, U.S.A.): *Journal of Sedimentary Research*, v. 72, p. 673–686,  
872 doi:10.1306/021802720673.
- 873 Bishop, J.L. et al., 2018a, Potential high priority subaerial environments for Mars sample return:  
874 *Proceedings of the Second International Mars Sample Return Conference*, v. 2071,  
875 doi:2018LPICo2071.6043I.
- 876 Bishop, J.L., Fairén, A.G., Michalski, J.R., Gago-duport, L., Baker, L.L., Velbel, M.A., Gross,  
877 C., and Rampe, E.B., 2018b, Surface clay formation during short-term warmer and wetter  
878 conditions on a largely cold ancient Mars: *Nature Astronomy*, v. 2, p. 206–213,  
879 doi:10.1038/s41550-017-0377-9.
- 880 Bishop, J.L., Gross, C., Danielsen, J., Parente, M., Murchie, S.L., Horgan, B., Wray, J.J.,  
881 Viviano, C., and Seelos, F.P., 2020, Multiple mineral horizons in layered outcrops at  
882 Mawrth Vallis, Mars, signify changing geochemical environments on early Mars: *Icarus*, v.  
883 341, p. 113634, doi:10.1016/j.icarus.2020.113634.
- 884 Bishop, J.L., Loizeau, D., Mckeown, N.K., Saper, L., Dyar, M.D., Des, D.J., Parente, M., and  
885 Murchie, S.L., 2013, What the ancient phyllosilicates at Mawrth Vallis can tell us about  
886 possible habitability on early Mars: *Planetary and Space Science*, v. 86, p. 130–149,  
887 doi:10.1016/j.pss.2013.05.006.
- 888 Bishop, J.L., and Rampe, E.B., 2016, Evidence for a changing Martian climate from the  
889 mineralogy at Mawrth Vallis: *Earth and Planetary Science Letters*, v. 448, p. 42–48,  
890 doi:10.1016/j.epsl.2016.04.031.
- 891 Broz, A.P., 2020, Organic Matter Preservation in Ancient Soils of Earth and Mars: *Life*, v. 10,  
892 doi:doi:10.3390/life10070113.
- 893 Broz, A.P., Clark, J., Archer, P.D., Sutter, B., Ming, D.W., Tu, V.M., Silva, L.C.R., and Horgan,  
894 B.H., 2021a, Thermal and Evolved Gas Analysis of Mars-analog Paleosols, *in* *Lunar and*  
895 *Planetary Science Conference*, v. 2136, p. 5–6.
- 896 Broz, A.P., Clark, J.V., Archer, P., Sutter, B., Tu, V.M., Silva, L.C.R., and Horgan, B.H.N.,  
897 2021b, Radiocarbon dating of Mars-analog paleosols reveals contamination with exogenous  
898 organic carbon, *in* *Terrestrial Analogs*, v. 8094.

- 899 Cannon, K.M., Sutter, B., Ming, D.W., Boynton, W. V., and Quinn, R., 2012, Perchlorate  
900 induced low temperature carbonate decomposition in the Mars Phoenix Thermal and  
901 Evolved Gas Analyzer (TEGA): *Geophysical Research Letters*, v. 39, p. 2–6,  
902 doi:10.1029/2012GL051952.
- 903 Carter, J., Loizeau, D., Mangold, N., Poulet, F., and Bibring, J., 2015, Widespread surface  
904 weathering on early Mars : A case for a warmer and wetter climate: *Icarus*, v. 248, p. 373–  
905 382, doi:10.1016/j.icarus.2014.11.011.
- 906 Danielson, J., Bishop, J., Usabel, G.S., Miura, J., Sessa, A., Wray, J., Itoh, Y., Parente, M.,  
907 and Murchie, S., 2019, Characterization of outcrops containing “doublet” spectra at  
908 Mawrth Vallis, Mars: *Lunar and Planetary Science Conference*, v. 2019, p. 1–179,  
909 doi:10.1029/2008g.
- 910 Dynarski, K.A., Bossio, D.A., and Scow, K.M., 2020, Dynamic Stability of Soil Carbon:  
911 Reassessing the “Permanence” of Soil Carbon Sequestration: *Frontiers in Environmental*  
912 *Science*, v. 8, doi:10.3389/fenvs.2020.514701.
- 913 Eigenbrode, J.L. et al., 2018, Organic matter preserved in 3-billion-year-old mudstones at Gale  
914 crater, Mars: *Science*, v. 360, p. 1096–1101, doi:10.1126/science.aas9185.
- 915 Ewing, S.A., Macalady, J.L., Warren-Rhodes, K., McKay, C.P., and Amundson, R., 2008,  
916 Changes in the soil C cycle at the arid-hyperarid transition in the Atacama Desert: *Journal*  
917 *of Geophysical Research*:, v. 113, p. 1–16, doi:10.1029/2007JG000495.
- 918 Finke, N. et al., 2019, Mesophilic microorganisms build terrestrial mats analogous to  
919 Precambrian microbial jungles: *Nature Communications*, v. 10, p. 1–11,  
920 doi:10.1038/s41467-019-11541-x.
- 921 Fornaro, T., Steele, A., and Brucato, J.R., 2018, Catalytic/protective properties of martian  
922 minerals and implications for possible origin of life on mars: *Life*, v. 8, p. 1–41,  
923 doi:10.3390/life8040056.
- 924 François, P., Szopa, C., Buch, A., Coll, P., Mcadam, A.C., Mahaffy, P.R., Freissinet, C., Glavin,  
925 D.P., and Cabane, M., 2015, Magnesium sulfate as a key mineral for the detection of  
926 organic molecules on Mars using pyrolysis: *Journal of Geophysical Research – Planets*, p.  
927 61–74, doi:10.1002/2015JE004884.Received.
- 928 Freissinet, C. et al., 2015, Organic molecules in the Sheepbed Mudstone, Gale Crater, Mars:  
929 *Journal of Geophysical Research : Planets*, v. 120, p. 495–514,  
930 doi:10.1002/2014JE004737.Received.
- 931 Fremd, T.J., 1996, Data Quality in Terrestrial Assemblages: Perspectives from Volcaniclastic  
932 Sequences of the John Day Basin, Oregon: *The Paleontological Society Special*  
933 *Publications*, v. 8, p. 131–131, doi:10.1017/s2475262200001337.
- 934 Gay, A., and Grandstaff, D.E., 1980, Chemistry and mineralogy of precambrian paleosols at  
935 Elliot Lake, Ontario, Canada: *Precambrian Research*, v. 12, p. 349–373.
- 936 Goesmann, F. et al., 2017, The Mars Organic Molecule Analyzer (MOMA) Instrument:  
937 Characterization of Organic Material in Martian Sediments: *Astrobiology*, v. 17, p. 655–  
938 685, doi:10.1089/ast.2016.1551.
- 939 Hays, L.E., Graham, H. V., Des Marais, D.J., Hausrath, E.M., Horgan, B., McCollom, T.M.,  
940 Parenteau, M.N., Potter-McIntyre, S.L., Williams, A.J., and Lynch, K.L., 2017,

- 941 Biosignature Preservation and Detection in Mars Analog Environments: *Astrobiology*, v.  
942 17, p. 363–400, doi:10.1089/ast.2016.1627.
- 943 Homann, M. et al., 2018, Microbial life and biogeochemical cycling on land 3,220 million years  
944 ago: *Nature Geoscience*, v. 11, p. 665–671, doi:10.1038/s41561-018-0190-9.
- 945 Horgan, B.H.N., 2013, Climate change and a sequence of habitable ancient surface environments  
946 preserved in pedogenically altered sediments at Mawrth Vallis, Mars., *in* *Lunar and*  
947 *Planetary Science Conference*, p. 3059.
- 948 Horgan, B., 2016, Strategies for Searching for Biosignatures in Ancient Martian Sub-Aerial  
949 Surface Environments: *Biosignature Preservation and Detection in Mars Analog*  
950 *Environments*, p. 7463, doi:10.1089/ast.2016.1627.
- 951 Horgan, B.H.N., Anderson, R.B., Dromart, G., Amador, E.S., and Rice, M.S., 2020, The mineral  
952 diversity of Jezero crater : Evidence for possible lacustrine carbonates on Mars: *Icarus*, v.  
953 339, p. 113526, doi:10.1016/j.icarus.2019.113526.
- 954 Horgan, B., Bishop, L., Christensen, P.R., and Bell, J.F., 2012, Potential ancient soils preserved  
955 at Mawrth Vallis from comparisons with Eastern Oregon paleosols: Implications for Early  
956 Martian Climate: *Third Conference on Early Mars*, v. 7074, p. 12–13.
- 957 Horgan, B., Rutledge, A., and Rampe, E., 2018, Clay mineralogy and crystallinity as a climatic  
958 indicator: Evidence for both cold and temperate conditons on early Mars: *46th Lunar and*  
959 *Planetary Science Conference*, p. 3–4, doi:10.1029/2006.
- 960 Ivanov, M.A., Slyuta, E.N., Grishakina, E.A., and Dmitrovskii, A.A., 2020, Geomorphological  
961 Analysis of ExoMars Candidate Landing Site Oxia Planum: *Solar System Research*, v. 54,  
962 p. 1–14, doi:10.1134/S0038094620010050.
- 963 Kleber, M., Bourg, I.C., Coward, E.K., Hansel, C.M., Myneni, S.C.B., and Nunan, N., 2021,  
964 Dynamic interactions at the mineral–organic matter interface: *Nature Reviews Earth and*  
965 *Environment*, v. 2, p. 402–421, doi:10.1038/s43017-021-00162-y.
- 966 Kleber, M., Mikutta, R., Torn, M., and Jahn, R., 2005, Poorly crystalline mineral phases protect  
967 organic matter in acid subsoil horizons: *European Journal of Soil Science*, p. 717–725,  
968 doi:10.1111/j.1365-2389.2005.00706.x.
- 969 Kremer, B., Kaźmierczak, J., and Środoń, J., 2017, Cyanobacterial-algal crusts from Late  
970 Ediacaran paleosols of the East European Craton: *Precambrian Research*,  
971 doi:10.1016/j.precamres.2017.12.018.
- 972 Krull, E.S., and Retallack, G.J., 2000,  $^{13}\text{C}$  depth profiles from paleosols across the Permian-  
973 Triassic boundary : Evidence for methane release: *GSA Bulletin*, v. 112, p. 1459–1472.
- 974 Kurth, V.J., MacKenzie, M.D., and DeLuca, T.H., 2006, Estimating charcoal content in forest  
975 mineral soils: *Geoderma*, v. 137, p. 135–139, doi:10.1016/j.geoderma.2006.08.003.
- 976 De la Rosa, J.M., González-Pérez, J.A., González-Vázquez, R., Knicker, H., López-Capel, E.,  
977 Manning, D.A.C., and González-Vila, F.J., 2008, Use of pyrolysis/GC-MS combined with  
978 thermal analysis to monitor C and N changes in soil organic matter from a Mediterranean  
979 fire affected forest: *Catena*, v. 74, p. 296–303, doi:10.1016/j.catena.2008.03.004.
- 980 Lantz, C., Poulet, F., Loizeau, D., Riu, L., Pilorget, C., Carter, J., Dypvik, H., Rull, F., and  
981 Werner, S.C., 2020, Planetary Terrestrial Analogues Library project: 1. characterization of

- 982 samples by near-infrared point spectrometer: *Planetary and Space Science*, v. 189, p.  
983 104989, doi:10.1016/j.pss.2020.104989.
- 984 Lawrence, C.R., Schulz, M.S., Masiello, C.A., Chadwick, O.A., and Harden, J.W., 2021, The  
985 trajectory of soil development and its relationship to soil carbon dynamics: *Geoderma*, v.  
986 403, doi:10.1016/j.geoderma.2021.115378.
- 987 Lehmann, J., and Kleber, M., 2015, The contentious nature of soil organic matter: *Nature*, p. 1–9,  
988 doi:10.1038/nature16069.
- 989 Lewis, J.M.T. et al., 2021, Pyrolysis of Oxalate, Acetate, and Perchlorate Mixtures and the  
990 Implications for Organic Salts on Mars: *Journal of Geophysical Research: Planets*, v. 126,  
991 doi:10.1029/2020JE006803.
- 992 Liivamägi, S., Rodoñ, J., Bojanowski, M., Gerdes, A., Stanek, J.J., Williams, L., and Szczerba,  
993 M., 2018, Paleosols on the Ediacaran basalts of the East European Craton: a unique record  
994 of paleoweathering with minimum diagenetic overprint: *Precambrian Research*,  
995 doi:10.1016/j.precamres.2018.07.020.
- 996 Liu, J., He, H., Michalski, J., Cuadros, J., Yao, Y., Tan, W., Qin, X., Li, S., and Wei, G., 2020,  
997 Reflectance spectroscopy applied to clay mineralogy and alteration intensity of a thick  
998 basaltic weathering sequence in Hainan Island, South China: *Applied Clay Science*, p.  
999 105923, doi:10.1016/j.clay.2020.105923.
- 1000 Liu, J., Michalski, J.R., Tan, W., He, H., Ye, B., and Xiao, L., 2021a, Anoxic chemical  
1001 weathering under a reducing greenhouse on early Mars: *Nature*,  
1002 doi:<https://doi.org/10.1038/s41550-021-01303-5>.
- 1003 Liu, J., Michalski, J.R., and Zhou, M., 2021b, Intense subaerial weathering of eolian sediments  
1004 in Gale crater, Mars: *Science Advances*, v. 7, doi:DOI: 10.1126/sciadv.abh2687.
- 1005 Loizeau, D. et al., 2020, ExoMars 2020 Surface Mission: Choosing a Landing Site: v. 2019, p.  
1006 2019–2020.
- 1007 Loizeau, D., Mangold, N., Poulet, F., Bibring, J., Bishop, J.L., Michalski, J., and Quantin, C.,  
1008 2015, History of the clay-rich unit at Mawrth Vallis, Mars: High-resolution mapping of a  
1009 candidate landing site: *Journal of Geophysical Research: Planets*, p. 1820–1846,  
1010 doi:10.1002/2015JE004894.Received.
- 1011 Loizeau, D., Quantin-nataf, C., Carter, J., Flahaut, J., Thollot, P., Lozac, L., and Millot, C., 2018,  
1012 Quantifying widespread aqueous surface weathering on Mars: The plateaus south of  
1013 Coprates Chasma: *Icarus*, v. 302, p. 451–469, doi:10.1016/j.icarus.2017.11.002.
- 1014 Mahaffy, P.R. et al., 2012, The sample analysis at Mars investigation and instrument suite: *Space*  
1015 *Science Reviews*, v. 170, p. 401–478, doi:10.1007/s11214-012-9879-z.
- 1016 Marin-Spiotta, E., Chaopricha, N.T., Plante, A.F., Diefendorf, A.F., Mueller, C.W., Grandy,  
1017 A.S., and Mason, J.A., 2014, Long-term stabilization of deep soil carbon by fire and burial  
1018 during early Holocene climate change: *Nature Geoscience*, v. 7, p. 428–432,  
1019 doi:10.1038/ngeo2169.
- 1020 Matthewman, R., Cotton, L.J., Martins, Z., and Sephton, M.A., 2012, Organic geochemistry of  
1021 late Jurassic paleosols (Dirt Beds) of Dorset, UK: *Marine and Petroleum Geology*, v. 37,  
1022 p. 41–52, doi:10.1016/j.marpetgeo.2012.05.009.

- 1023 Mcadam, A., Sutter, B., Archer, P., Franz, H., and Eigenbrode, J., 2020a, The chemistry and  
1024 mineralogy of the Glen Torridon clay-bearing unit from Mars Science Laboratory Sample  
1025 Analysis at Mars: 51st Lunar and Planetary Science Conference, v. 2243, p. 60–74.
- 1026 Mcadam, A.C., Sutter, B., Archer, P.D., Franz, H.B., Wong, G.M., Lewis, J.M.T., Eigenbrode,  
1027 J.L., and Stern, J.C., 2020b, Constraints on the Mineralogy and Geochemistry of Vera  
1028 Rubin Ridge, Gale Crater, Mars, From Mars Science Laboratory Sample Analysis at Mars  
1029 Evolved Gas Analyses: *Journal of Geophysical Research: Planets*, p. 1–26,  
1030 doi:10.1029/2019JE006309.
- 1031 Miller, K.B., McCahon, T.J., and West, R.R., 1996, Lower Permian (wolfcampian) paleosol-  
1032 bearing cycles of the U.S. Midcontinent: Evidence of climatic cyclicity: *Journal of*  
1033 *Sedimentary Research*, v. 66, p. 71–84, doi:10.1306/D42682B6-2B26-11D7-  
1034 8648000102C1865D.
- 1035 Ming, D.W. et al., 2014, Volatile and Organic Compositions of Sedimentary Rocks in  
1036 Yellowknife Bay, Gale Crater, Mars: *Science Express*, p. 1–15,  
1037 doi:10.1126/science.1245267.
- 1038 Nabhan, S., Wiedenbeck, M., Milke, R., and Heubeck, C., 2016, Biogenic overgrowth on detrital  
1039 pyrite in ca. 3.2 Ga Archean paleosols: *Geology*, v. 44, p. 763–766, doi:10.1130/G38090.1.
- 1040 Nelson, P.N., and Baldock, J.A., 2005, Estimating the molecular composition of a diverse range  
1041 of natural organic materials from solid-state C NMR and elemental analyses:  
1042 *Biogeochemistry*, v. 72, p. 1–34, doi:10.1007/s10533-004-0076-3.
- 1043 Noe Dobrea, E.Z., McAdam, A.C., Freissinet, C., Franz, H., Belmahdi, I., Hammersley, M.R.,  
1044 and Stoker, C.R., 2016, Characterizing the mechanisms for the preservation of organics at  
1045 the Painted Desert: Lessons for MSL, Exo-Mars, and Mars 2020: 47th Lunar and Planetary  
1046 Science Conference, p. Abstract #2796.
- 1047 Otto, A., Shunthirasingham, C., and Simpson, M.J., 2005, A comparison of plant and microbial  
1048 biomarkers in grassland soils from the Prairie Ecozone of Canada: *Organic Geochemistry*,  
1049 v. 36, p. 425–448, doi:10.1016/j.orggeochem.2004.09.008.
- 1050 PiPujol, M.D., and Buurman, P., 1994, The distinction between ground-water gley and surface-  
1051 water gley phenomena in Tertiary paleosols of the Ebro basin, NE Spain: *Palaeogeography,*  
1052 *Palaeoclimatology, Palaeoecology*, v. 110, p. 103–113, doi:10.1016/0031-0182(94)90112-0.
- 1053 Plante, A.F., Fernández, J.M., Haddix, M.L., Steinweg, J.M., and Conant, R.T., 2011, Biological,  
1054 chemical and thermal indices of soil organic matter stability in four grassland soils: *Soil*  
1055 *Biology and Biochemistry*, v. 43, p. 1051–1058, doi:10.1016/j.soilbio.2011.01.024.
- 1056 Poulet, F., Gross, C., Horgan, B., Loizeau, D., Bishop, J.L., Carter, J., and Orgel, C., 2020,  
1057 Mawrth Vallis, Mars: A Fascinating Place for Future In Situ Exploration: *Astrobiology*, v.  
1058 20, p. 1–36, doi:10.1089/ast.2019.2074.
- 1059 Ramirez, R.M., Kopparapu, R., Zugger, M.E., Robinson, T.D., Freedman, R., and Kasting, J.F.,  
1060 2014, Warming early Mars with CO<sub>2</sub> and H<sub>2</sub>: *Nature Geoscience*, v. 7, p. 59–63,  
1061 doi:10.1038/ngeo2000.
- 1062 Rampe, E., Morris, R. V, Ruff, S.W., Dehouck, E., Achilles, C.N., Ming, D.W., Bish, D.L., and  
1063 Chipera, S.J., 2014, Amorphous phases on the surface of Mars: Eighth International  
1064 Conference on Mars, p. 1–2.

- 1065 Raynaud, X., and Nunan, N., 2014, Spatial ecology of bacteria at the microscale in soil: PLoS  
1066 ONE, v. 9, doi:10.1371/journal.pone.0087217.
- 1067 Reardon, P.N., Chacon, S.S., Walter, E.D., Bowden, M.E., Washton, N.M., and Kleber, M.,  
1068 2016, Abiotic Protein Fragmentation by Manganese Oxide: Implications for a Mechanism  
1069 to Supply Soil Biota with Oligopeptides: *Environmental Science and Technology*, v. 50, p.  
1070 3486–3493, doi:10.1021/acs.est.5b04622.
- 1071 Retallack, G.J., 2016, Astropedology: palaeosols and the origins of life: *Geology Today*, v. 32, p.  
1072 172–178, doi:10.1111/gto.12149.
- 1073 Retallack, G.J., 2014, Paleosols and paleoenvironments of early Mars: *Geology*, v. 42, p. 755–  
1074 758, doi:10.1130/G35912.1.
- 1075 Retallack, G.J., 2019, *Soil of the Past*: Wiley Blackwell.
- 1076 Retallack, G.J., Bestland, E., and Fremd, T., 2000, Eocene and Oligocene Paleosols of Central  
1077 Oregon: *Geological Society of America Special Paper*, v. 344, p. 1–192,  
1078 doi:10.1046/j.1365-3091.2001.0394c.x.
- 1079 Retallack, G.J., and Krull, E.S., 1999, Landscape ecological shift at the Permian – Triassic  
1080 boundary in Antarctica: *Australian Journal of Earth Sciences*, v. 46, p. 785–812.
- 1081 Retallack, G.J., and Mao, X., 2019, Paleoproterozoic ( ca . 1 . 9 Ga ) megascopic life on land in  
1082 Western Australia: *Palaeogeography, Palaeoclimatology, Palaeoecology*, v. 532, p. 109266,  
1083 doi:10.1016/j.palaeo.2019.109266.
- 1084 Retallack, G.J., and Noffke, N., 2019, Are there ancient soils in the 3 . 7 Ga Isua Greenstone Belt  
1085 , Greenland ? *Palaeogeography, Palaeoclimatology, Palaeoecology*, v. 514, p. 18–30,  
1086 doi:10.1016/j.palaeo.2018.10.005.
- 1087 Retallack, G.J., Wynn, J.G., and Fremd, T.J., 2004, Glacial-interglacial-scale paleoclimatic  
1088 change without large ice sheets in the Oligocene of central Oregon: *Geology*, v. 32, p. 297–  
1089 300, doi:10.1130/G20247.1.
- 1090 Rye, R., and Holland, H., 2000, Life associated with a 2 . 76 Ga ephemeral pond ? : Evidence  
1091 from Mount Roe # 2 paleosol: *Geology*, v. 28, p. 483–486, doi:10.1130/0091-  
1092 7613(2000)28<483:LAWAGE>2.0.CO;2.
- 1093 Schiller, M., Dickinson, W., Ditchburn, R.G., Graham, I.J., and Zondervan, A., 2009,  
1094 Atmospheric  $^{10}\text{Be}$  in an Antarctic soil: Implications for climate change : *Journal of*  
1095 *Geophysical Research*, v. 114, p. 1–8, doi:10.1029/2008jf001052.
- 1096 Schmidt, M.W.I. et al., 2011, Persistence of soil organic matter as an ecosystem property:  
1097 *Nature*, doi:10.1038/nature10386.
- 1098 Sheldon, N.D., Retallack, G.J., and Tanaka, S., 2015, Geochemical Climofunctions from North  
1099 American Soils and Application to Paleosols across the Eocene - Oligocene Boundary in  
1100 Oregon Geochemical Climofunctions from North American Soils and Application to  
1101 Paleosols across the Eocene-Oligocene Boundary in Or: *The Journal of Geology*, v. 110, p.  
1102 687–696, doi:10.1086/342865.
- 1103 Smith, R., and Horgan, B.H.N., 2021, Nanoscale Variations in Natural Amorphous and  
1104 Nanocrystalline Weathering Products in Mafic to Intermediate Volcanic Terrains on Earth :  
1105 Implications for Amorphous Detections on Mars: *Journal of Geophysical Research: Planets*,

- 1106 v. 126, p. 1–30, doi:10.1029/2020JE006769.
- 1107 Smith, R., Horgan, B., Rampe, E., and Dehouck, E., 2018a, The Composition of Amorphous  
1108 Phases in Soils and Sediments on Earth and Mars: 49th Lunar and Planetary Science  
1109 Conference 2018, p. 14–15.
- 1110 Smith, R.J., Rampe, E.B., Horgan, B.H.N., and Dehouck, E., 2018b, Deriving Amorphous  
1111 Component Abundance and Composition of Rocks and Sediments on Earth and Mars:  
1112 *Journal of Geophysical Research: Planets*, v. 123, p. 2485–2505,  
1113 doi:10.1029/2018JE005612.
- 1114 Stern, J.C., Sutter, B., Freissinet, C., Navarro-González, R., Mckay, C., and Archer, P.D., 2015,  
1115 Evidence for indigenous nitrogen in sedimentary and aeolian deposits from the Curiosity  
1116 rover investigations at Gale ...: *PNAS*, doi:10.1073/pnas.1420932112.
- 1117 Sutter, B., Boynton, W. V., Ming, D.W., Niles, P.B., Morris, R. V., Golden, D.C., Lauer, H. V.,  
1118 Fellows, C., Hamara, D.K., and Mertzman, S.A., 2012, The detection of carbonate in the  
1119 martian soil at the Phoenix Landing site: A laboratory investigation and comparison with  
1120 the Thermal and Evolved Gas Analyzer (TEGA) data: *Icarus*, v. 218, p. 290–296,  
1121 doi:10.1016/j.icarus.2011.12.002.
- 1122 Sutter, B., Mcadam, A., Mahaffy, P., Ming, D., Edgett, K., Rampe, E., Eigenbrode, J., Franz,  
1123 H., and Freissinet, C., 2017, Evolved gas analyses of sedimentary rocks and eolian  
1124 sediment in Gale Crater, Mars: Results of the Curiosity rover's sample analysis at Mars  
1125 instrument from Yellowknife Bay to the Namib Dune: *Journal of Geophysical Research :*  
1126 *Planets*, p. 2574–2609, doi:10.1002/2016JE005225.
- 1127 Sweeney, K.E., Roering, J.J., and Ellis, C., 2015, Experimental evidence for hillslope control of  
1128 landscape scale: *Science*, v. 349, p. 51–53, doi:10.1126/science.aab0017.
- 1129 Szopa, C. et al., 2020, First Detections of Dichlorobenzene Isomers and Trichloromethylpropane  
1130 from Organic Matter Indigenous to Mars Mudstone in Gale Crater , Mars : Results from the  
1131 Sample Analysis at Mars Instrument Onboard the Curiosity Rover: v. 20, p. 292–306,  
1132 doi:10.1089/ast.2018.1908.
- 1133 Viviano-Beck, C.E. et al., 2014, Revised CRISM spectral parameters and summary products  
1134 based on the currently detected mineral diversity on Mars: *Journal of Geophysical*  
1135 *Research: Planets*, v. 119, p. 1403–1431, doi:10.1002/2014JE004627.
- 1136 Watanabe, Y., Martin, J.E., and Ohmoto, H., 2000, Geochemical evidence for terrestrial  
1137 ecosystems 2.6 billion years ago: *Nature*, v. 408, doi:10.1038/35046052.
- 1138 Watanabe, Y., Stewart, B.W., and Ohmoto, H., 2004, Organic- and carbonate-rich soil formation  
1139 ~2.6 billion years ago at Schagen, East Transvaal district, South Africa: *Geochimica et*  
1140 *Cosmochimica Acta*, v. 68, p. 2129–2151, doi:10.1016/j.gca.2003.10.036.
- 1141 Williams, E.K., Fogel, M.L., Berhe, A.A., and Plante, A.F., 2018, Distinct bioenergetic  
1142 signatures in particulate versus mineral-associated soil organic matter: *Geoderma*, v. 330, p.  
1143 107–116, doi:10.1016/j.geoderma.2018.05.024.
- 1144 Ye, B., and Michalski, J.R., 2021, Precipitation-Driven Pedogenic Weathering of Volcaniclastics  
1145 on Early Mars: *Geophysical Research Letters*, v. 48, p. 1–10, doi:10.1029/2020GL091551.
- 1146
- 1147